

STOLLED  
# N-99922

68 85 102

368 ↓

THE IONOSPHERE DIRECT MEASUREMENTS SATELLITE  
INSTRUMENTATION (EXPLORER VIII)

CODE 5

by

↓ R. E. Bourdeau, J. L. Donley,  
and E. C. Whipple, Jr. [1961] 56p 2 refs  
NASA Goddard Space Flight Center, Greenbelt, Md.

50840

(NASA TMX [REDACTED])

[9] conf

61-173-1867

Presented at the Natl. IAS/ARS Joint Meeting, Los Angeles, June 13-16, 1961

National IAS }  
ARS } ..... Joint Meeting

THE IONOSPHERE DIRECT MEASUREMENTS SATELLITE  
INSTRUMENTATION (EXPLORER VIII)

by

R. E. Bourdeau, J. L. Donley,  
and E. C. Whipple, Jr.

NASA Goddard Space Flight Center

ABSTRACT

The Ionosphere Direct Measurements Satellite (Explorer VIII) is described with emphasis on the physics of experiments designed to measure electron density (rf impedance probe), electron temperature (electron temperature probe), positive ion concentration (ion current monitor), ion mass (retarding potential probe). Also discussed are experiments designed to measure the momentum, energy and spatial distribution of dust particles. Experimental data typical of that processed to date are presented.

The methods used by systems engineers to fulfill the special requirements imposed by the scientific experiments upon the overall satellite design are described. Data such as the satellite's thermal and spin decay history are reported.

Of particular importance to spacecraft technologists interested in the influence of the earth's magnetic field upon satellite orientation are measurements obtained from the scientific experiments on the effect of potential differences observed at various points on the satellite surface. Finally, a new method for the determination of satellite aspect is introduced.

## INTRODUCTION

The Ionosphere Direct Measurements Satellite (Explorer VIII) was launched by a Juno II vehicle (Figure 1) from Cape Canaveral on 3 November 1960, into an orbit with an inclination of  $50^{\circ}$ , a perigee of 425 kilometers and an apogee of 2300 kilometers. It had a planned active life of two months.

As the name implies, the primary mission of the Ionosphere Direct Measurements Satellite was the acquisition of data on the properties of charged particles with thermal energies, a group which exerts the greatest influence on communications. As the name further implies, the measurements were made by techniques which depend on sampling the spacecraft's local environment with data transmitted over the telemetry link. Thus, the satellite differs from other US ionosphere satellites where the ionospheric parameters are obtained indirectly from ground-based observations of the arrival characteristics of radio signals transmitted from the spacecraft.

The ionospheric parameters measured on Explorer VIII were the electron concentration ( $N_e$ ) and temperature ( $T_e$ ) and the positive ion concentration ( $N_+$ ) and mass ( $M_+$ ). These data were obtained by the use of five separate experiments, two being used for electron temperature.

Since a body moving at high velocities modifies the characteristics of an ionized medium through which it travels, it was recognized that the extent of this modification had to be known in order to derive meaningful geophysical quantities from the ionospheric experiments. Specifically, it was felt important to know the behavior of four quantities as a function of the spacecraft orientation relative to the velocity, magnetic field and solar vectors. These are: the potential ( $\phi$ ) which develops between the satellite and the medium as a result

of their mutual interaction, the electron current  $(i_e)_s$  and positive ion current  $(i_+)_s$  flowing from the medium to the satellite, and the photo current  $(i_p)_s$  due to emission from the satellite surfaces of electrons produced by solar radiation. The subscript s refers to current values as observed at the skin of the spacecraft. As it turned out, measurements of these four quantities permitted the development of a model of the plasma sheath which formed around the satellite.

It is not possible to develop a model of the plasma sheath entirely from the five geophysical experiments. Consequently, two additional scientific experiments were added to fulfill this requirement. The following is a list of the seven experiments flown on Explorer VIII to accomplish the primary objective:

<u>Experiment</u>	<u>Ionospheric Parameter</u>	<u>Sheath Parameter</u>
1. RF Impedance Probe	$N_e$	
2. Ion Current Monitor	$N_+$	$(i_+)_s$
3. Retarding Potential Probe	$M_+$	
4. Two-Element Electron Temperature Probe	$T_e$	$(i_e)_s, \phi$
5. Three-Element Electron Temperature Probe	$T_e$	$\phi$
6. Electron Current Monitor		$(i_e)_s + (i_p)_s$
7. Total Current Monitor		$(i_e)_s + (i_+)_s$ $+ (i_p)_s$

Because the orders of magnitude of the ion, electron and photoemission currents were estimated before launch to be comparable it was decided that if possible they should be measured separately. In particular, experience with the results of Langmuir probes in rockets where the ion and electron currents were not separated led to

uncertainties in measured electron temperatures. For these reasons, five of the six current sensors (Experiments 2 - 7) were all constructed so as to perform an in-situ separation of currents, while the sixth one measured the net or total current to a representative satellite area. The latter served both as a check on the other sensors and as a calibration monitor.

Another geophysical objective of Explorer VIII was the study of the characteristics of interplanetary dust particles. Two independent systems, a microphone and a photomultiplier tube, together determined the momentum, the energy, and the spatial distribution of the particles.

The tenth and last experiment involved the use of a rotating shutter device designed to measure the electric field produced by the plasma sheath which forms about the satellite. This was a secondary objective.

All ten experiments require a knowledge of the orientation of the satellite in space. A solar-horizon system was included for this purpose. Finally, in order to perform second-order corrections to the data, the temperature at four points on the satellite was measured.

The successful operation of ten experiments functioning continuously for two months from a chemical power supply with a limitation on payload weight of only 90 pounds requires delicate and complex instrumentation. The requirement dictated by the rocket booster for a 450 rpm spin rate during the launch phase introduced a need for an orbital despin device. This, in addition to experimental requirements for separation of the last stage rocket plus the need to extend a shortened dipole

probe made the satellite design problem even more difficult.

This report starts with a description of the ten experiments. In some cases, the explanation of the derivation from measured quantities of the desired parameters is facilitated by illustrative examples of experimental data obtained during the satellite's active life. Next presented is a description of the instrumentation including the method of telemetry encoding. The mechanical features primarily thermal control, the despin and the dipole release mechanisms are described briefly. Results related to spacecraft technology are reported. These include a model of the electrical interaction between the satellite and the ionized atmosphere, some data on the effects of the earth's magnetic field on satellite orientation and the satellite's thermal history.

#### LOCATION OF COMPONENTS

Photographs of the Explorer VIII Satellite are presented in Figures 2, 3 and 4. The aluminum shell consists of two truncated cones joined at the equator by a cylinder. The spacecraft is 30 inches in diameter at the equator and 30 inches high. The weight including the fourth-stage separation mechanism is 90 pounds.

In Figure 2, are located the following components: the two-element electron temperature probe, the electron and total current monitors, all containing protective covers; the sun-horizon aspect sensor; the despin mechanism, and the two micrometeorite microphone sounding boards.

In Figure 3, a view  $180^{\circ}$  opposite from Figure 2, are located the following components: the three-element electron temperature probe; the ion current

monitor and the retarding potential sensor, all containing protective covers; the micrometeorite photomultiplier; the quadriloop telemetry antenna; and thermal coatings located on the upper and lower cones in a pattern conducive to the maintenance of an equipotential surface.

In Figure 4, the satellite is shown with the top cone removed. As shown, the power supply consists of eight packs containing mercury batteries. Solar cells were not used because asymmetric charging on their surfaces could adversely affect the scientific results.

Also shown in Figure 4 is the electronic instrumentation column surmounted by the electric field meter which is located on and at the most forward end of the spin axis. The sensor for the rf impedance probe experiment was a shortened-dipole antenna each half of which was 10 feet long. The reel containing these two wires which were extended after satellite injection is mounted around the electronic instrumentation column container.

#### THE RADIO-FREQUENCY IMPEDANCE PROBE EXPERIMENT

The objective of this experiment was the measurement of electron concentration. This is accomplished by comparing the in-flight capacitance ( $C$ ) of the sensor with its free-space value ( $C_0$ ). The sensor, located on the satellite's equator is a shortened dipole antenna, each half of which is 10 feet long. The capacitance  $C_0$  is measured before flight by use of a half shell fabricated to the satellite configuration and one of the two antenna wires. The cut is made through the spin-axis and the half-shell is then placed on the appropriate ground plane.

The experiment was tested previously in vertical sounding rockets<sup>1</sup>. The electron concentration is

computed from the Appleton-Hartree formula which relates  $N_e$  to the dielectric constant (K) of the medium. Specifically,

$$K = \frac{C}{C_o} = 1 - \frac{81N_e}{f^2} \quad (1)$$

where  $f$  is the frequency (6.5 Mc) of the voltage applied to the antenna probe. It should be emphasized that the amount of radiated power is negligibly small.

Since  $C_o$  is measured before flight and  $f$  is known, it is necessary only to measure  $C$  in order to compute  $N_e$ . The method of measuring  $C$  is illustrated schematically in Figure 5. The heart of the system is an oscillator whose frequency is determined in part by a sweep generator and in part by the capacitance of the sensor. The start of the sweep is triggered by an 80-millisecond square wave developed from a gate contained within the telemetry system. A crystal filter delivers an output pulse to the computer each time the oscillator is tuned to 6.5 Mc. Two such pulses occur every 80 milliseconds because the sweep generator output has an up and down sweep. The time intervals from the start of the sweep to the occurrence of the two pulses are a measure of the probe capacitance and are presented to the telemetry system by the computer in digital form. Since a measurement of  $C$  is made every 40 milliseconds, the experiment can, in principle, search out ionospheric heterogeneities with dimensions as small as 300 meters.

#### THE ION CURRENT MONITOR

The geophysical objective of this experiment, illustrated schematically in Figure 6, is the measurement of positive ion concentration. The sensor, constructed in planar geometry, consists of three

parallel electrodes. The outer grid is flush with and electrically connected to the satellite skin. Thus, it acts as an electrostatic shield by preventing potentials on the inner electrode from disturbing the plasma sheath which surrounds the satellite. The inner grid is biased negatively to remove incoming electron current and to suppress photoemission from the collector. Consequently, the collector current ( $i_+$ ) contains only the contribution of positive ions.

Since the satellite's velocity ( $V$ ) is much larger than that of the positive ions,  $i_+$  will be a maximum when the angle ( $\theta$ ) between the sensor and the direction of motion is a minimum. Specifically, for small angles

$$i_+ = \alpha_+ N_+ e V \cos \theta, \quad (2)$$

where  $\alpha_+$  is the effective electrical transparency of the two grids and  $e$  is the electronic charge.

Because of weight limitations, the use of the electrometer is time-shared with the retarding potential and the two-element electron temperature probe experiments by means of a mechanical commutator. One of the commutator switches connects the ion current monitor's collector to the electrometer input (point A, in the Figure 6 schematic) for 30 seconds of each 90-second interval. At the same time, a second switch (point C) connects the electrometer return and the shield braid of the coaxial cable to satellite potential. During each 30-second interval, a third switch (point B) changes the system sensitivity in three steps of 10 seconds each by successive application of three separate collector load resistors. Such a range switch is necessary because the ion concentration can change from  $10^6/\text{cm}^3$  at perigee down to  $10^3/\text{cm}^3$  at apogee.

The electrometer uses 100 percent feedback, a feature which provides three important characteristics to the system. First, it insures long term stability. Less than one-percent drift was observed during environmental testing when the system was operated for two weeks in a vacuum while the package temperature was cycled between 0° and 50°C. Secondly, feedback keeps the collector at satellite potential, irrespective of the voltage drop across the collector load resistor. Thirdly, the feedback permits the sensor to be located remotely from the mechanical commutator and the electrometer. This is because it brings about an "effective" short circuit between the center conductor and the shield braid of the interconnecting coaxial cable thus eliminating the effects of the latter's resistive and capacitive leakage.

A typical result obtained from the ion current monitor experiment at an altitude of 1000 km is presented in Figure 7, where  $i_+$  is plotted as a function of the azimuth angle between the sensor and the velocity and solar vectors. The absence of current when the sensor was pointed at the sun is experimental evidence that suppression of photoemission was successfully accomplished. As expected,  $i_+$  has its maximum value when  $\theta$  is a minimum. The ion concentration computed from this result was  $1.3 \times 10^4/\text{cm}^3$ , a value consistent with the electron concentration measured at the same time by the RF probe.

#### THE RETARDING POTENTIAL EXPERIMENT

The objective of this experiment, illustrated schematically in Figure 8, is the measurement of the mass ( $M_+$ ) of the positive ions. The sensor is physically identical to the ion current monitor. It differs electrically in that a potential varying between -3 and +20 volts in 0.2 seconds is applied to the collector.

As described above, the use of the electrometer is time-shared with the ion current monitor and the two-element electron temperature probe experiments, each experiment being on for 30 seconds during each 90-second interval. As with the ion current monitor, three sensitivity ranges on for 10 seconds each are used. The retarding potential is applied at the electrometer return and to the shield braid by a switch located at point C.

An actual volt-ampere curve taken during the flight of Explorer VIII is presented in Figure 9. Since the satellite is traveling much faster than the positive ions, it follows that the ions will have a kinetic energy relative to the satellite proportional to their mass. Specifically, the potential of the collector relative to the plasma required to retard one-half the ions of a given mass is given by

$$\phi_{cp} = \phi_{cs} + \phi = \frac{M_+ (V \cos \theta)^2}{2e}, \quad (3)$$

where  $\phi_{cs}$  is the collector-to-satellite potential which in Figure 9 is that required to reduce  $i_+$  to one-half its maximum value, and  $\phi$  is the potential of the satellite relative to the medium as measured by the electron temperature probes.

When the current in Figure 9 is at one-half the saturation value, the angle between the trap and the velocity vector is  $28^\circ$ , and collector potential,  $\phi_{cs}$ , is 3.7 volts. Substitution of these values into Equation 3 together with the known values of satellite potential (-0.1 volt) and velocity ( $7.4 \times 10^5$  cm/sec) yields a value of 16 AMU for the positive ion mass which identifies it as  $O^+$ .

## THE TWO-ELEMENT ELECTRON TEMPERATURE EXPERIMENT

A schematic drawing of the two-element electron temperature experiment is presented in Figure 10. The sensor consists of only two electrodes, a grid flush with the satellite skin and a collector. The collector is biased positively to remove photoemission and incoming ion current from the measured collector current. Electron temperature is computed by plotting the collector current on a logarithmic scale as a function of a variable potential (-1.2 to +8v.) applied to the grid. A typical result is shown in Figure 11. The shape of the curve is in good agreement with Langmuir probe theory. Two distinct slopes in the regions where the grid is below and above plasma potential are apparent. The slope of the curve when the potential is negative is a measure of the electron temperature which for the case illustrated was  $1800^{\circ} \pm 300^{\circ}\text{K}$  with the uncertainty due to the limited resolution. It is also possible to obtain from the curve a measurement of the potential of the satellite relative to the plasma at the sensor location. This is generally taken as the negative value of either the point where the curve departs from this slope or the point of intersection of the two slopes. For the actual case shown, a satellite potential between 0 and - 0.15 volts is obtained.

The sweep voltage was removed from the grid and the grid returned to satellite potential on alternate 30-second operation modes of the experiment by the mechanical commutator. During these modes any disturbance of the sheath due to the presence of the sweep voltage on the outer surface of the satellite could be determined. Analysis of the data shows that no large disturbance was present.

## THE ELECTRON CURRENT MONITOR

As discussed in the introduction, two supporting scientific experiments were added to assist in the development of a model of the plasma sheath surrounding the satellite. One of these, the electron current monitor is illustrated schematically in Figure 12. It is mechanically identical to the ion current monitor but differs electrically in that the inner grid is biased positively rather than negatively. The positive bias serves to remove incoming ion current from the measured collector current. In this case, the collector current contains contribution from both photoemission and incoming electron current and is given by

$$i = \alpha_e (i_e)_s + \alpha_p (i_p)_s , \quad (4)$$

where  $\alpha_e$  and  $\alpha_p$  are the respective grid transparencies.

The measured collector current is plotted in Figure 13 as a function of aspect for one spin period. The current has a maximum positive value (photoemission) when the azimuth angle of the sensor relative to the sun is zero. On the shaded side of the satellite, the electron current is varying as function of the azimuth angle from the point corresponding to the direction of the cross-product of the velocity and magnetic field vectors ( $\vec{v} \times \vec{B}$ ) in the satellite coordinate system. The maximum current is observed when this angle is a minimum. This effect agrees with the prediction of Beard and Johnson<sup>2</sup>. It is due to the fact that the motion of the satellite through the earth's magnetic field caused an induced potential on the satellite surface. The most positive point on the satellite surface occurs at the point corresponding to the  $\vec{v} \times \vec{B}$  direction.

As illustrated in Figure 12, the use of electrometer #2 is time-shared equally between the electron current monitor, the three-element electron temperature experiment, and the total current monitor in a manner similar to the time sharing of electrometer #1.

#### THE THREE-ELEMENT ELECTRON TEMPERATURE EXPERIMENT

The three-element electron temperature experiment is illustrated schematically in Figure 14. Here, the outer grid is kept at the satellite potential. The inner grid is biased positively, thus removing the effects of positive ions. The collector current is then studied as a function of a variable potential applied to the collector. This device is sensitive to photoemission so that only volt-ampere curves taken when the sensor is not sunlit are applicable. Otherwise, the principles are the same as for the two-electrode probe. There is one important geophysical observation which can be made by comparing results from the two types of Langmuir probes. The three-electrode probe measures the temperature of only those electrons energetic enough to overcome the satellite potential which is generally negative. Consequently, if the two methods are in agreement which was generally true it is an indication that the electron energy distribution is Maxwellian.

#### THE TOTAL CURRENT MONITOR

The total current to the satellite was measured at its equator by the sensor illustrated in Figure 15. It consists simply of a collector flush with and insulated from the satellite skin, with the collector current given by

$$i = i_t = (i_e)_s + (i_+)_s + (i_p)_s \quad (5)$$

It represents then, the sum of the effects of Figures 7 and 13 except that the overall amplitude of each component is larger since no grid transparencies are involved. The total current at the point of measurement is larger since no grid transparencies are involved.

The total current at the point of measurement is plotted as a function of aspect in Figure 16. It is in definite agreement with the general features of the graphs in Figures 7 and 13. Specifically, the current peaks in the positive direction when the solar angle is a minimum because of photoemission. It also peaks in the positive direction for a velocity azimuth angle near zero. The peak here is due to the "ram effect" upon which the positive ion current is largely dependent. The displacement from the zero angle point is due to the influence of the electron current in this region. Finally, a peak electron current occurs when the angle between the sensor and the vector  $\vec{V} \times \vec{B}$  approaches a minimum.

It can be seen that the six experiments using the two electrometers required that the latter be zero-centered, that is capable of measuring either an electron or ion current. Also time sharing required that the electrometer's dynamic range be such that it measure currents as low as  $3 \times 10^{-10}$  amperes as needed by the ion current monitor at apogee altitudes and as high as  $10^{-5}$  as needed by the electron temperature probe at perigee when the probe's grid is at plasma potential.

## THE MICROMETEORITE EXPERIMENTS

Explorer VIII contained two separate experiments to measure properties of micron size interplanetary dust particles. Both sensors obtained information by detection of particles impacting on a special surface. One detector was a piezoelectric crystal attached to each of two sounding boards (Figures 2 and 3) acoustically isolated from the payload. Present calibration information indicates that this sensor measures a quantity related to the momentum of the particle.

The second detector used a photomultiplier tube (Figure 3) which was made opaque by evaporating a coating of Al on the face of the tube. When a dust particle impacted on this surface at hypervelocities, the sensor measured the electromagnetic radiation lying within the spectral response of the sensor. Calibration of this sensor, including using micron size particles at 10 km/sec, has demonstrated that particles of mass greater than  $10^{-13}$  gm are detectable.

Information from the microphone sensors was obtained in three different sensitivity levels. This data was stored in three independent digital counters whose storage capability was 64, 8, and 4. The photomultiplier data was in analog form and real time only. The information contained in the analog pulse was three different light energy sensitivity levels and data of radiation background.

Information concerning the mass distribution of particles of mass  $10^{-13}$  gm  $\leq$  m  $\leq$   $10^{-8}$  gm in the vicinity of the earth was obtained and is being analyzed. The distribution of particle momentum determined by the microphone sensors appears to be quite significant, especially when compared to similar data from other satellites.

## THE ELECTRIC FIELD METER EXPERIMENT

The objective of the field meter experiment is the measurement of the distribution of charge which accumulates on the satellite surface due to interactions with the ionosphere. The sensor, shown in Figure 17, is located at the forward end of the spin axis and is termed a rotating-shutter type electric field meter. It consists of two basic elements: an exposed four-bladed motor-driven shutter (rotor) grounded to the satellite skin by brushes and a four-bladed stator or sensor located directly behind and having the same configuration as the rotor. The stator which is returned to ground through a resistive load is alternately exposed and shielded by the rotor whose speed is controlled at 7500 rpm. The driving motor is equipped with special lubrication-free bearings and high-altitude brushes to insure operation in a vacuum environment.

The electric field meter is designed to measure the electric field due to the plasma sheath which forms around the satellite. The electric field is proportional to the ratio of the satellite potential relative to the medium and the thickness of the sheath. Since the medium is ionized, the electric field meter also is sensitive to the net current which flows between the medium and the satellite. The signals due to the electric field ( $V_E$ ) and to the diffusion current ( $V_J$ ) are in quadrature and can be separated by phase discrimination. Their amplitudes are given by

$$V_E = \epsilon EA\omega R$$

and

$$V_J = JAR$$

where  $\epsilon$  is a constant,  $A$  is the area of the stator,  $\omega$  is the angular rotor frequency,  $R$  is the stator resistive load, and  $J$  is the net diffusion current

density.

As shown in Figure 18, a synchronous wave is developed at the back end of the sensor. This signal is used for the motor control servo and the synchronous rectifier for the measurement of  $V_E$ . The total output ( $V_T$ ) is given by

$$V_T = (V_E^2 + V_J^2)^{1/2}$$

The experiment will measure fields up to 10,000 volts per meter with a noise equivalent of less than 10 volts/meter. The residual field drift due to rotor-to-stator contact potential is also less than 10 volts/meter. The exposed surfaces of the field meter are gold plated and the rotor to stator spacing is 3 mm.

Due to the large power demand (3 watts) and limited mechanical lifetime of the driving motor, the experiment is turned on by command from the ground. The outputs are time shared into the telemetry system during "on" time by the mechanical commutator. The experiment is automatically turned off after two minutes operation by a command program module.

#### INSTRUMENTATION

As with all satellites, only a small percentage of the total Explorer VIII weight could be devoted to actual instrumentation. The weight distribution of the major systems is as follows:

Structure and Mechanical Systems	34 lbs.
Batteries	34 lbs.
Wiring and Connectors	3 lbs.
Sensors	5 lbs.
Instrumentation	12 lbs.

A photograph of the instrumentation column is presented in Figure 19. The supporting instrumentation includes a separation timer, aspect instrumentation, computers, a telemetry system and transmitter, and a command receiver. To compress these plus circuitry directly associated with ten scientific experiments into a column weighing only twelve pounds requires a considerable amount of planning effort. The most complex part of the scientific instrumentation is that associated with the six experiments illustrated schematically in Figures 6, 8, 10, 12, 14 and 15. These experiments all share the use of the mechanical commutator, the sweep generator, and the two electrometers.

The mechanical commutator permits time-sharing for the six sensors of the two electrometers by use of solenoid-operated switches inserted between the sensor collectors and the electrometers. It simultaneously permits time-sharing for the pertinent sensors of the use of the sweep generator. Its third function is that of range switching. The commutator has a 90-second repetitive program consisting of 9 ten-second intervals derived from a transistorized multivibrator which actuates the solenoid. As indicated by the schematics of the individual experiments, this program is shown in Table 1.

TABLE 1

## MECHANICAL COMMUTATOR PROGRAM

TIME (sec)	ELECTROMETER #1 Telemeter channels 5, 9, 13	ELECTROMETER #2 Telemeter channels 6, 10, 14
0-10	Retarding Potential Probe Low Sensitivity	Three-Element Electron Temperature Probe Low Sensitivity
10-20	Retarding Potential Probe Medium Sensitivity	Three-Element Electron Temperature Probe Medium Sensitivity
20-30	Retarding Potential Probe High Sensitivity	Three-Element Electron Temperature Probe High Sensitivity
30-40	Ion Current Monitor Low Sensitivity	Electron Current Monitor Low Sensitivity
40-50	Ion Current Monitor Medium Sensitivity	Electron Current Monitor Medium Sensitivity
50-60	Ion Current Monitor High Sensitivity	Electron Current Monitor High Sensitivity
60-70	Two-Element Electron Temperature Probe Low Sensitivity	Total Current Monitor Low Sensitivity
70-80	Two-Element Electron Temperature Probe Medium Sensitivity	Total Current Monitor Medium Sensitivity
80-90	Two-Element Electron Temperature Probe High Sensitivity	Total Current Monitor High Sensitivity

The commutator is unique in that special volumetric guarding techniques allows switching of currents as low as  $10^{-10}$  amperes without difficulties due to either resistive or capacitive effects. In the flight of Explorer VIII, it performed over a half-million operations at the time the satellite ceased transmitting.

The sweep generator develops a repetitive wave with a period of 0.2 seconds and has three taps: from -3 to +20 volts applied to the retarding potential (Figure 8) and three-element electron temperature probe (Figure 14) experiments; from -1.2 to +8 volts applied to the two-element electron temperature probe (Figure 10); and a two-volt output which is telemetered. A low output impedance (10K ohms) was used to prevent current flowing from the medium from affecting the pertinent electrode potentials.

The aspect system used in the Explorer VIII satellite consists of a combination solar and horizon sensing unit. The solar portion consists of two slits behind each of which was located a photo-sensitive silicon diode. One slit is parallel to the spin axis, and the other is slanted at approximately 25 degrees. The horizon portion consists of two diodes behind small apertures appropriately located. The horizon and solar sensors share common instrumentation which measured the time of an indication to within five milliseconds. The source of the indication is identified by the magnitude of the signal received by the pertinent diode. Measurement of the time between indications on the two solar slits compared to the roll period allows calculation of the angle between the sun vector and the spin axis. A similar determination of the angle between the spin axis and the satellite position vector is obtained from

horizon indications. The overall aspect system is designed to determine satellite orientation to an accuracy of one degree.

The data telemetry system operated continuously so that all data transmission was real time. The system is a descendant of that used in the Vanguard satellites. The transmitter output contains bursts of amplitude modulation separated by periods of no oscillation called blanks. The frequency within each tone burst is varied from 9 to 22.5 kc in either an analog or digital (eight discrete frequencies) form. The length of blanks is variable from 0.5 to 1.1 milliseconds. The average radiated power was 100 milliwatts at 108 megacycles. For data acquisition, the required pre-detection receiver bandwidth was 50 kc. For this value and a receiver antenna gain of 13 db, a predicted signal-to-noise ratio of 14 db was obtained at a 1500 mile range.

The basic element of time in the telemetry system, called a frame, is approximately 40 milliseconds in length and contains 16 alternate bursts and blanks with the sixteenth burst longer than the other bursts as a means of synchronization which serves to identify the start of a frame. Table 2 gives the telemetry allocations for each frame and identifies the bursts as digital or analog. The temperature at four separate locations on the payload was telemetered by means of four variable length blanks.

---

**TABLE 2**

---

**TELEMETRY CHANNEL ALLOCATIONS**  
**Explorer VIII Satellite**

---

<b>BURST</b>	<b>TYPE</b>	<b>INFORMATION</b>
1	Digital	Aspect Magnitude
2	Digital	Aspect Time
3	Digital	Micrometeorite Microphone
4	Digital	Micrometeorite Microphone
5	Analog	Electrometer #1
6	Analog	Electrometer #2
7	Analog	Sweep Generator Output
8	Analog	Micrometeorite Photomultiplier
9	Analog	Electrometer #1
10	Analog	Electrometer #2
11	Analog	Sweep Generator Output
12	Digital	RF Impedance Probe
13	Analog	Electrometer #1
14	Analog	Electrometer #2
15	Analog	Sweep Generator Output
16	Analog	Micrometeorite Photomultiplier

---

The command receiver together with the command program module turned on the electric field meter from the command transmitter signal and then turned the experiment off at the end of a two-minute interval. Except for the electric field meter experiment, all instrumentation operated continuously.

The chemical power supply on Explorer VIII was designed such that the scientific experiments would terminate simultaneously with rf transmissions as nearly as possible. This objective was achieved. Mercury cells were chosen because they have the highest ratio of power output per unit weight. Their main disadvantage is that their shelf life contributes significantly to their active life. This was overcome by close scheduling with the manufacturer.

#### MECHANICAL SYSTEMS

Due to the high rotational speed of 450 rpm required by the Juno II launch vehicle for injection accuracy, it was necessary to provide a system to despin the satellite after orbital injection and deploy the RF Impedance Probe. The final spin rate had to be sufficiently low such that collector current versus sweep voltage data from the electron temperature and retarding potential probes was independent of satellite orientation effects yet high enough for the payload to remain free of precession or tumbling during the two-month active lifetime.

The orbital injection sequence is shown in Figure 20. A battery operated timer actuated a release mechanism separating the payload from the fourth stage rocket and initiated the first stage despin device approximately two minutes after burnout. The two minute delay was chosen as a compromise between risk of "bumping" due to final stage after-burning and the desire to prevent payload

precession due to an unfavorable moment of inertia with the fourth stage bottle attached. The squib-fired first stage despin consisted of throwing away two weighted wires originally wrapped around the equator of the satellite. This stage was designed to decrease the payload spin rate from the launch value of 450 rpm to about 100 rpm. Release of the wires from the payload started the extension by centrifugal force of the RF Impedance Probe which simultaneously served as second stage despin. The probe consisted of two ten-foot flexible wires weighted at the ends which were stored on a spool within the payload prior to deployment. Rate of extension was governed at one foot per second by means of a mechanical brake arrangement. The final orbital spin rate of 22.1 rpm was well within the overall design criteria. The spin rate of the satellite had decayed to only 21.4 rpm at the end of one month.

The satellite was designed to maintain stability about the spin axis. Favorable moments of inertia were obtained by locating batteries near the periphery of the payload. The moment of inertia about the spin axis was  $25.95 \text{ in-lb-sec}^2$  while the maximum and minimum transverse moments of inertia were 20.89 and 19.11  $\text{in-lb-sec}^2$ .

#### SOME RESULTS RELATED TO SPACECRAFT TECHNOLOGY

Of interest to the problem of tracking of spacecraft is the extent of the interaction of a vehicle and an ionized medium. From the data presented in Figures 7, 11, 13, and 16, it is possible to develop a model of one type of interaction, that of the plasma sheath immediately surrounding the body. This model is illustrated by Figure 21 for a daytime condition where the magnetic field is zero. The lack of a positive ion current in the satellite wake as exhibited

by Figure 7 supports the existence of an electron sheath immediately adjoining the satellite surface in the back of the satellite. If it is assumed that the electron sheath is in the form of a cone, its size may be estimated from the ratio of the satellite-to-ion velocities and the satellite diameter. In this case the cone has a half-angle of about  $25^\circ$  and extends back a distance of about one satellite radius. The slightly negative potential (0 to  $-.15$  volts) measured by the electron temperature probe supports the existence of a positive ion sheath which envelopes both the satellite and the electron wake. The thickness of the ion sheath would be comparable to one Debye length which is computed to be 2.5 cm. The remainder of the model describes the current exchange between the satellite and the medium. A positive ion current flows from the medium at angles from  $-90$  to  $+90$  degrees relative to the velocity vector peaking in the direction of the motion. The electron current flowing from the medium to the satellite is modulated to a lesser extent in accordance with the velocity vector. Finally, there is a photoemission current effective at angles of  $\pm 60^\circ$  relative to the sun, with a maximum density value of  $5 \times 10^{-9}$  amps/cm<sup>2</sup>. This latter value can be compared with the random electron current density to predict the altitude at which the satellite can be expected to go significantly positive. For most ionospheric models this will occur at about 4000 km, just above the apogee altitude of Explorer VIII.

The effect of the magnetic field is introduced in Figure 22. Here, as predicted by Beard and Johnson<sup>2</sup>, the motion of a satellite with velocity  $V$  through the magnetic field produces an induced potential difference over the

satellite surface given by

$$\phi = \phi_0 + (\vec{V} + \vec{B}) \cdot \vec{d}$$

where  $\phi_0$  would be the potential with no magnetic field and  $\vec{d}$  the vector distance of any point on the surface from the satellite center. The electron current would be expected to be a maximum where  $\phi$  is most positive which would be near the point corresponding to the direction  $\vec{V} \times \vec{B}$ . This prediction is consistent with the observations. At the equator, it was observed that the electron current peaked when the total current monitor pointed in the  $\vec{V} \times \vec{B}$  direction as the satellite spun. The modulation of the current at the equator due to magnetic field was higher than in the upper cone, as would be expected, since the change in distance from the  $\phi_0$  plane is greater. It is estimated that there existed approximately a 0.14 volt potential difference measured across the equator and a 0.04 volt potential difference measured at the top cone. As expected, all points in the direction  $\vec{V} \times \vec{B}$  were more positive than  $\phi_0$  and all other points correspondingly more negative.

The earth's magnetic field also affects the satellite orientation. This was observed on Explorer VIII as with other satellites. For this particular satellite, it caused a spin rate decay of about 3 percent in one month's time. It also caused the spin axis to move at a rate of about 2 degrees per day.

The use of the data from the ion trap together with the solar sensor to determine the satellite orientation is believed to be a significant contribution to spacecraft technology. The time of the peak ion current indicates when the angle between the trap and the velocity vector is a minimum, and since the velocity vector is known from orbital information, orientation can be computed.

This method has the advantage of being useful whenever the solar cell yields data, whereas the horizon sensor's usefulness was limited to local noon plus or minus about three hours. This kind of orientation sensor may have particular application on vehicles designed for re-entry into the earth's atmosphere where the angle of attack must be known.

Also of interest to spacecraft technologists is the thermal design employed. Proper operation of the payload instrumentation is guaranteed only when the temperature of the instrument column and battery packs is maintained between  $0^{\circ}\text{C}$  to  $50^{\circ}\text{C}$ . In order to meet these requirements the following steps were taken:

(1) The internal instruments and battery packs were insulated from the all aluminum structure by Kel-F spacers.

(2) A suitable ratio of emissivities on the outer skin surface is provided by a combination of surface sandblasting and the use of non-conducting iron oxide paint. As shown in Figures 2 and 3, the paint is applied in a pattern conducive to the maintenance of an equipotential surface.

(3) A good radiation exchange between the inner surfaces of the payload is obtained by coating interior surfaces with white titanium oxide, covering battery packs with aluminum foil, and polishing all other internal metallic parts. These provisions are evident in Figure 4.

The launch time was selected so that the satellite had an orientation with respect to the sun favorable for maintaining a good thermal balance during the active life time. Figure 23 gives the percentage time in sun-light for the orbit and the angle between the sun and satellite spin axis as a function of days after launch.

The satellite approached the 100 percent sunlight condition only at the end of its active life which was as predicted. The spin axis to sun angle was determined from the solar aspect sensor and shows that the sun was shining on the upper cone of the satellite only. This condition was not predicted and is due to the interaction between the payload and the earth's magnetic field which disturbed the spin axis orientation as discussed previously. However, this variation from predicted behavior was not serious enough to cause thermal problems in the payload.

The temperature of the satellite was monitored by means of thermistors at four locations: (1) center of the instrument column, (2) battery pack, (3) equatorial rim, and (4) meteorite photomultiplier. The temperature extremes at three of the locations measured during the active lifetime are: (1) instrument column, 22°C to 33°C; (2) battery pack, 17°C to 27°C; (3) skin, -3°C to 37°C.

#### ENVIRONMENTAL TESTING

Of extreme importance to satellite projects is the environmental testing phase. When optimized, the testing program results in a reliable payload developed through a minimum amount of testing. Minimum testing is urgent not only from the standpoint of economy but also to reduce the long lead times which experimenters face.

The testing program for all payloads using the Juno II booster involved the use of three prototypes and two flight payloads. A thermal prototype operated under vacuum temperature conditions is used to measure thermal conductivity. This in addition to emissivity measurements on the skin provides the basic

data from which the amount of thermal coatings are computed. An environmental prototype is subjected to vibration, shock, centrifuge, spin, and low vacuum temperature tests. The electrical prototype is used only for long lived temperature tests in a high vacuum. Prototype testing is performed at about 1.5 times expected flight levels. Both flight payloads are subjected to vibration, centrifuge, spin, all at levels lower than that expected in flight plus a long temperature test in high vacuum.

On the basis of experience gained in testing of the Explorer VIII payloads, it is considered that the test program described above is excessive. First since no failures were observed in the many shock, centrifuge and spin tests, it is felt that with proper attention to experience gained in construction techniques and choice of components these particular tests can be eliminated from future testing programs. The only failures occurred either under vibration or under temperature test at high vacuum. The experience shows also that failures are more apt to occur in the temperature-vacuum tests after components have been fatigued under vibration. Consequently, these tests should be done in series with vibration first rather than the parallel operation used in the Explorer VIII prototype testing. Thus one prototype can substitute for the electric and environmental prototypes.

Secondly, it was found that quality control on surface emissivity was difficult to maintain from one model to another. This makes the need for a thermal prototype questionable. It is felt that data permitting a rough design for thermal control can be used while the single prototype is undergoing vacuum-temperature

tests. Final touching up is then accomplished as a result of data obtained on the actual flight model.

Thirdly, it was found that a more reliable and expedient method of handling the flight models is to eliminate one and depend upon spare components. In this manner, more attention can be paid to the single flight unit and rarely will a replacement part have to be used.

A recommended test program for future use based on the Explorer VIII experience is as follows: First, test and evaluation personnel should determine by actual measurement, if necessary, the vibration amplitude and spectrum which the payload can be expected to experience. Secondly, a mechanical model with simulated components should be constructed and then tested for unusual responses to these vibration levels. Thirdly, a specification on the thermal constant design to maintain components generally between 0° and 50°C should be imposed. Fourthly, all suppliers then should subject their components individually first to vibration levels equal to expected values and then to high vacuum tests where the temperature is cycled 10° above and below the payload design values. In the cycling, it is just as important to maintain the extremes of temperature for long periods of time as it is to cycle. Finally, the prototype should be assembled and then subjected to 1.5 times the flight vibration levels followed only by the vacuum-temperature tests. Components which fail the first time should then be tested separately before proceeding with the tests.

For flight units, suppliers should construct two sets of components. The "spare" component should receive the flight vibration levels and vacuum-temperature testing. The other set of components are assembled into the flight model and subjected to flight levels and vacuum-

## REFERENCES

1. J. E. Jackson and J. A. Kane, "Performance of an RF Impedance Probe in the Ionosphere," J. Geophys. Research, 65 (1960) No. 7.
2. D. B. Beard and F. S. Johnson, "Charge and Magnetic Field Interaction with Satellites, " J. Geophys. Res., 65 (1960) No. 1

temperature testing.

#### ACKNOWLEDGMENTS

In addition to the authors, the ionospheric experimenters, all from the Space Sciences Division of the Goddard Space Flight Center, were: J. Kane and G. Serbu. The experimenters for the Micrometeorite Experiments were W. Alexander, O. Berg and C. McCracken, from the same division. W. Archer designed the Electric Field Meter Instrumentation; C. Hamilton acted as Project Coordinator. The following personnel from the Payloads Systems Division of GSFC provided the Instrumentation; D. Hepler, (Transmitter and Command Receiver); J. Shaffert, (Command Program); J. Albus, (Aspect); D. Schaefer, (Aspect and RF Probe Computers); J. Scobey, (Telemetry); W. Conant and D. Krueger, (Integration and Testing); R. Waddel, (Electrometers and Sweep Generator); H. Evans and T. Flatley, (Mechanical Design of the Electric Field Meter). C. Stout and A. Ferris of the Data Systems Division designed the Data Reduction System.

The Marshall Space Flight Center was responsible for launching the satellite. W. Greever was Project Engineer. The following personnel from its Guidance and Control Laboratory participated in the payload development: H. Wagner, (Mechanical Systems); E. Cagle and E. Berg, (Power Supply and Network Wiring); W. Harper, (Qualriloop Antenna); W. Snoddy, (Thermal Design); H. Schaefer, (Environmental Testing).

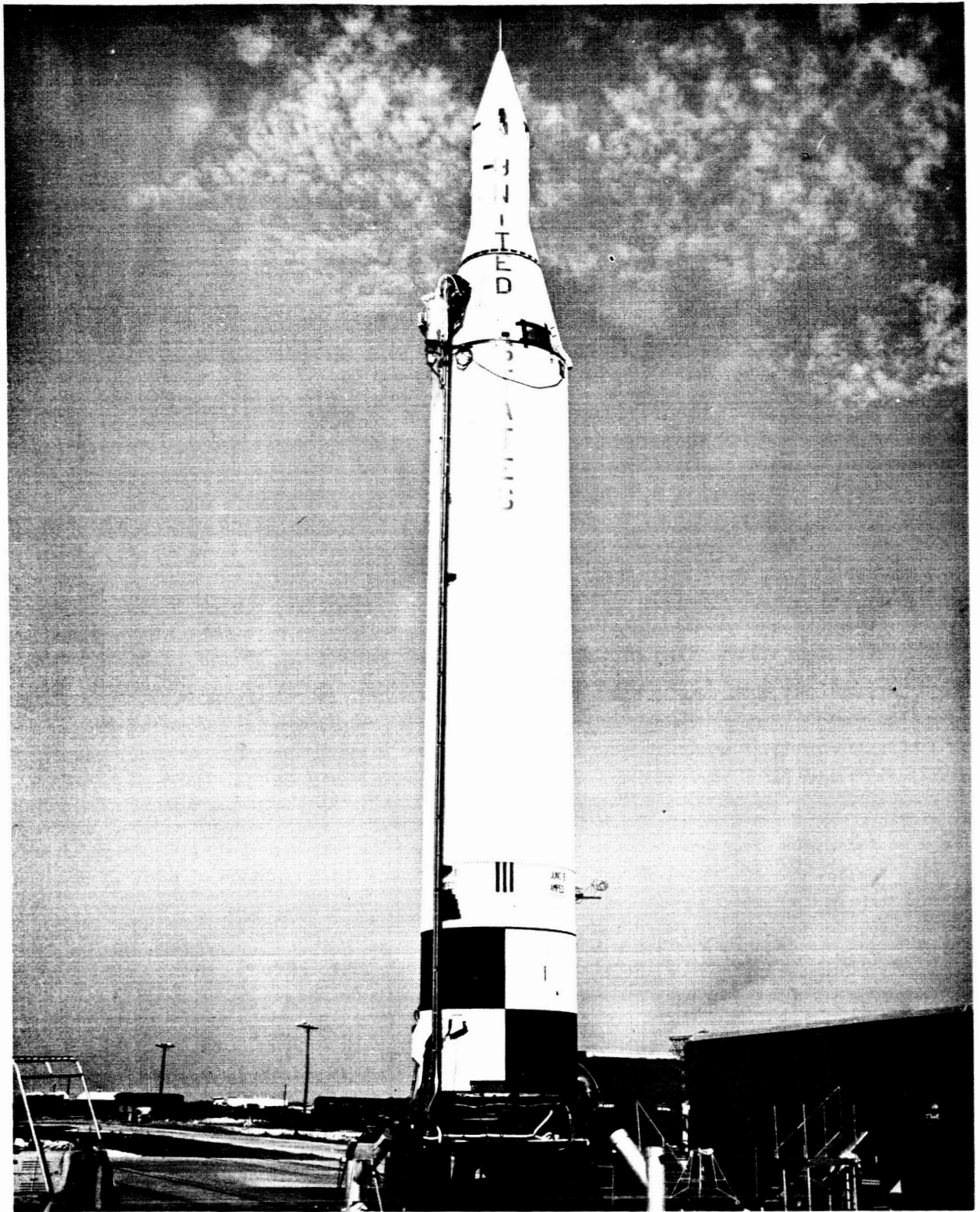
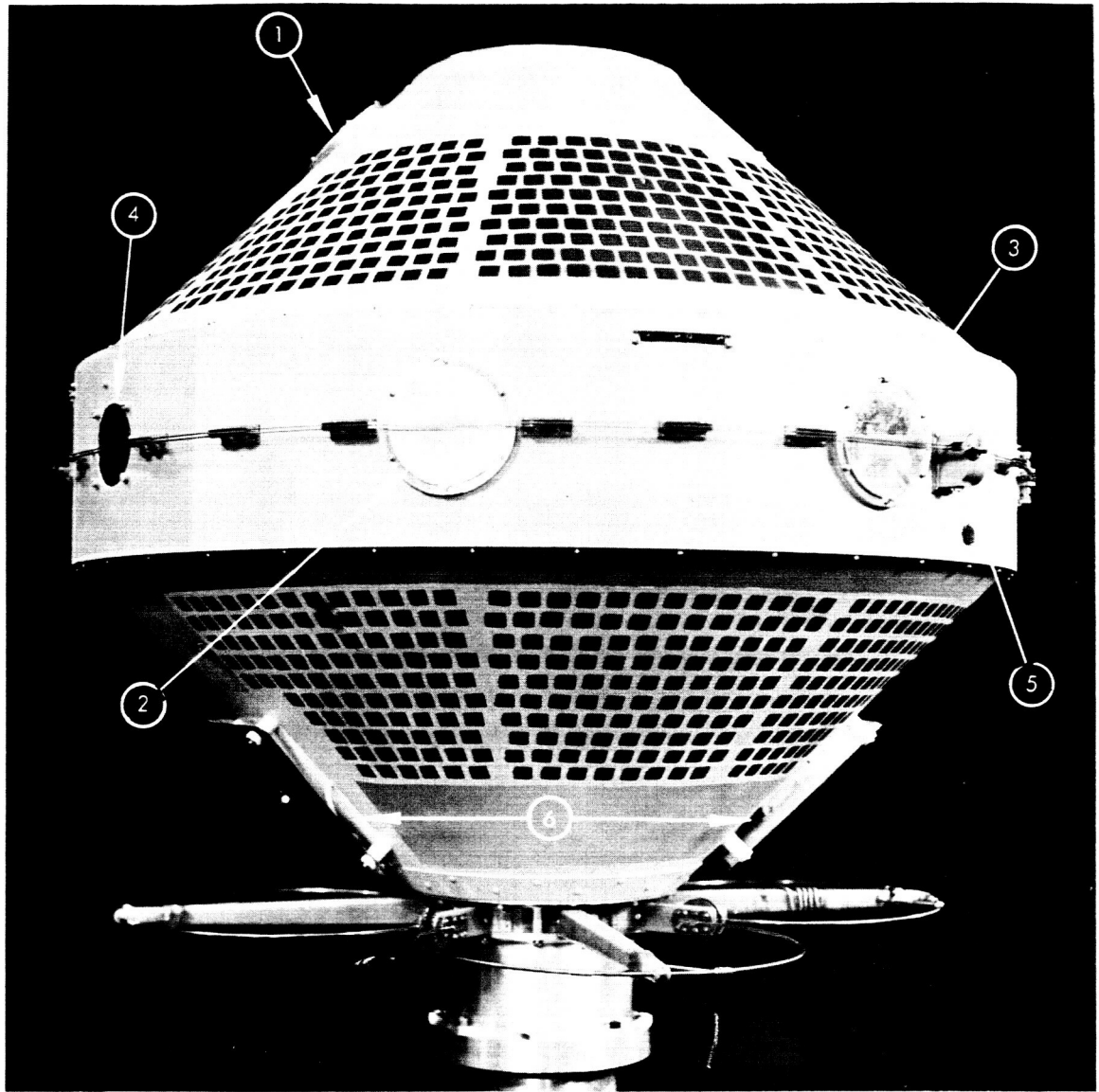
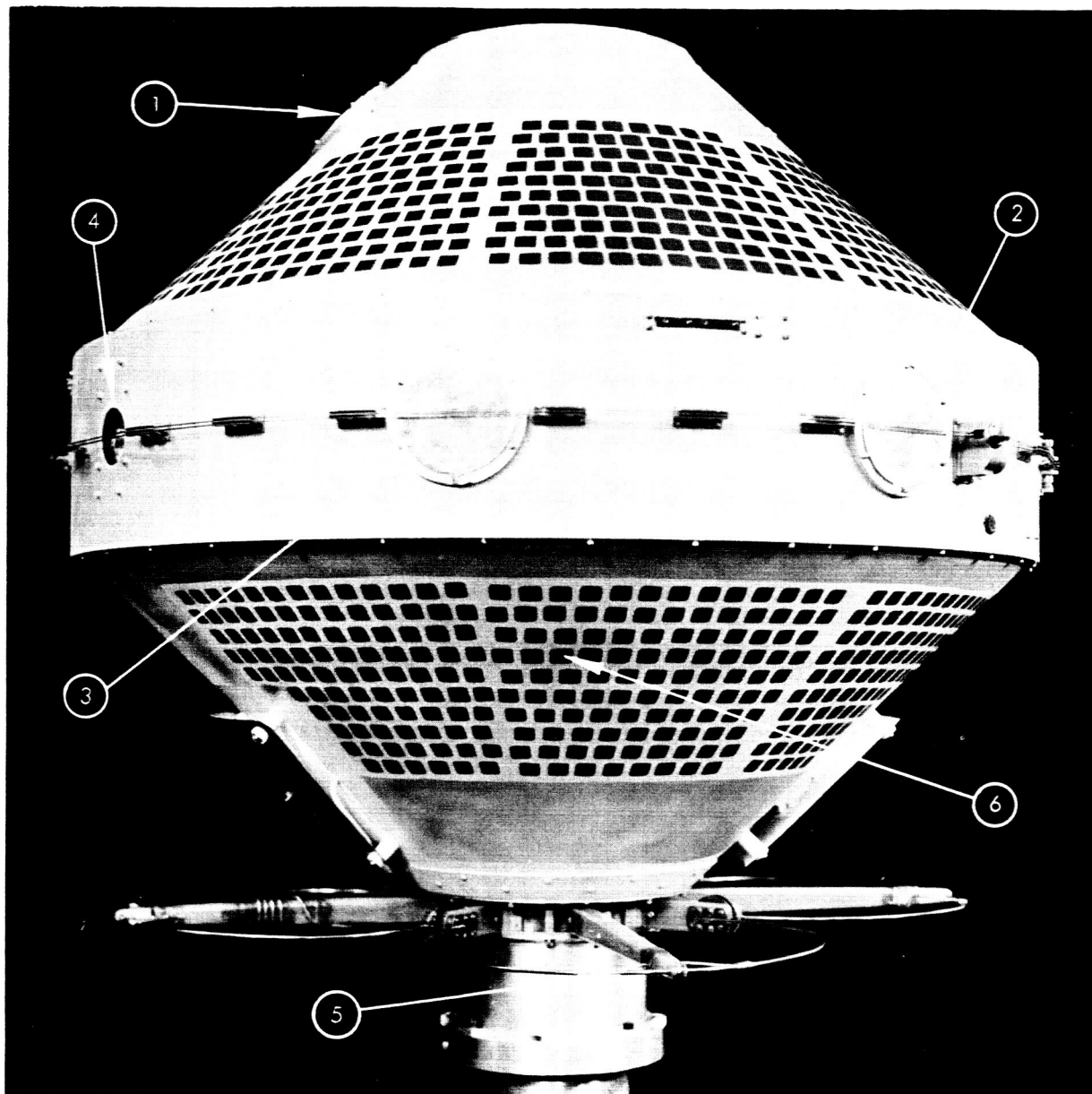


Figure 1. Juno II Launch Vehicle Containing Explorer VIII Satellite.



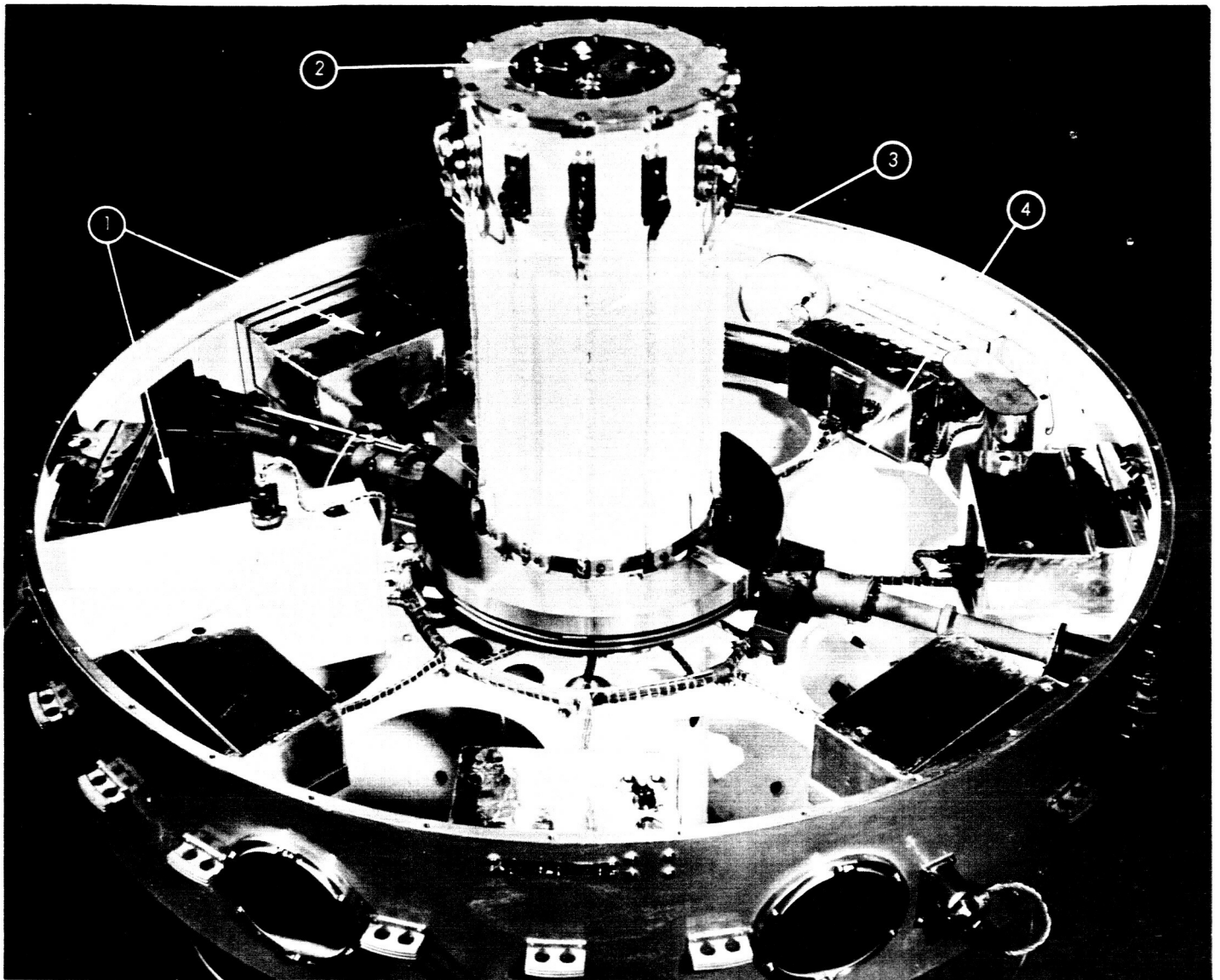
- 1 Two-Element Electron Temperature Probe
- 2 Total Current Monitor
- 3 Electron Current Monitor
- 4 Sun-Horizon Aspect Sensor
- 5 Despin Mechanism
- 6 Micrometeorite Microphone Sounding Boards

Figure 2. Explorer VIII Satellite, Showing Component Locations.



- 1 Three-Element Electron Temperature Probe
- 2 Ion Current Monitor
- 3 Retarding Potential Probe
- 4 Micrometeorite Photomultiplier
- 5 Telemetry Antenna
- 6 Thermal Coatings

Figure 3. Explorer VIII Satellite, Showing Component Locations.



- 1 Battery Packs
- 2 Electric Field Meter
- 3 Instrumentation Column Container
- 4 RF Impedance Probe Storage Reel and Release Mechanism

Figure 4. Explorer VIII Satellite With Top Cone Removed.

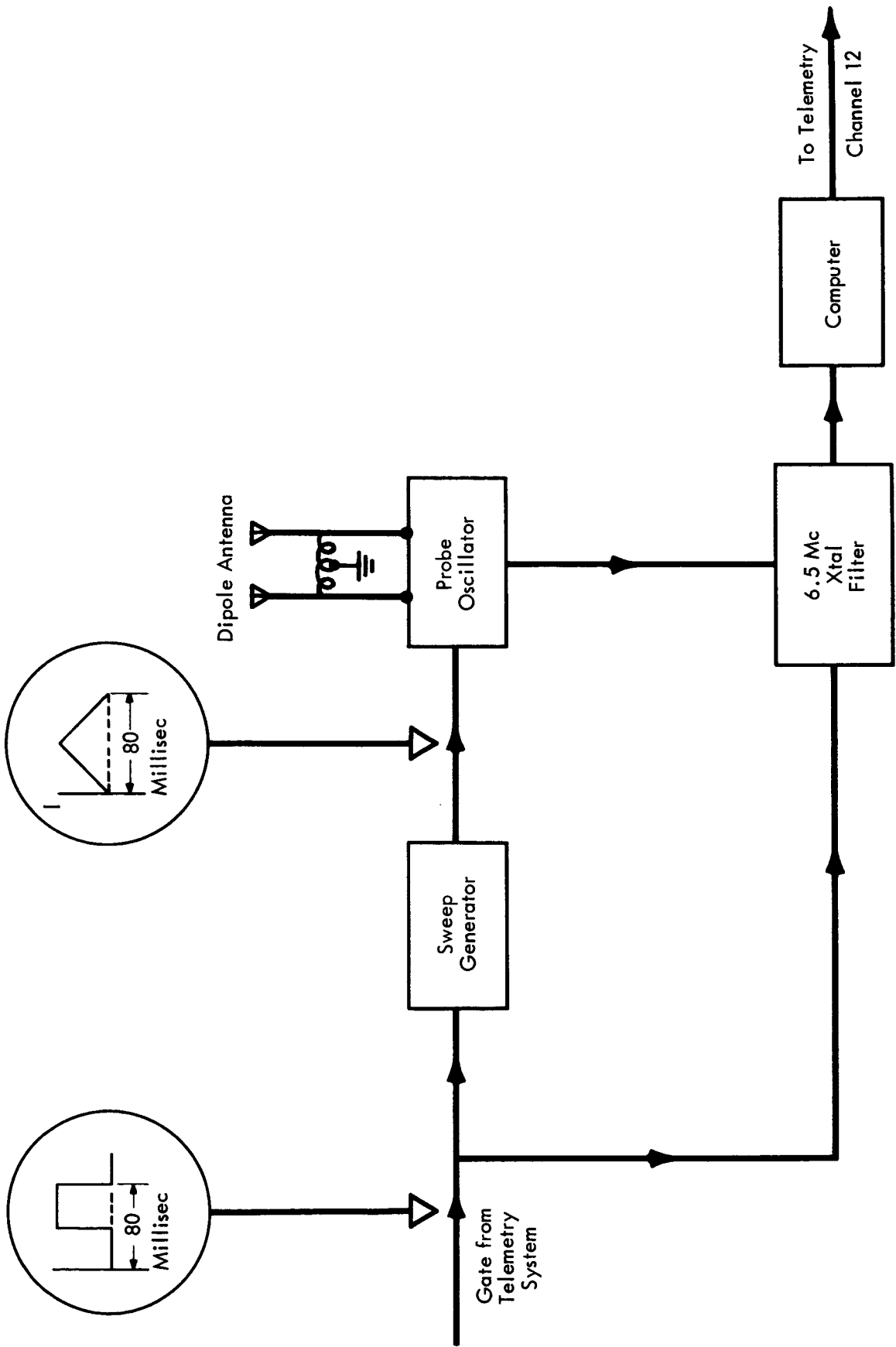


Figure 5. Block Diagram of RF Impedance Probe Experiment

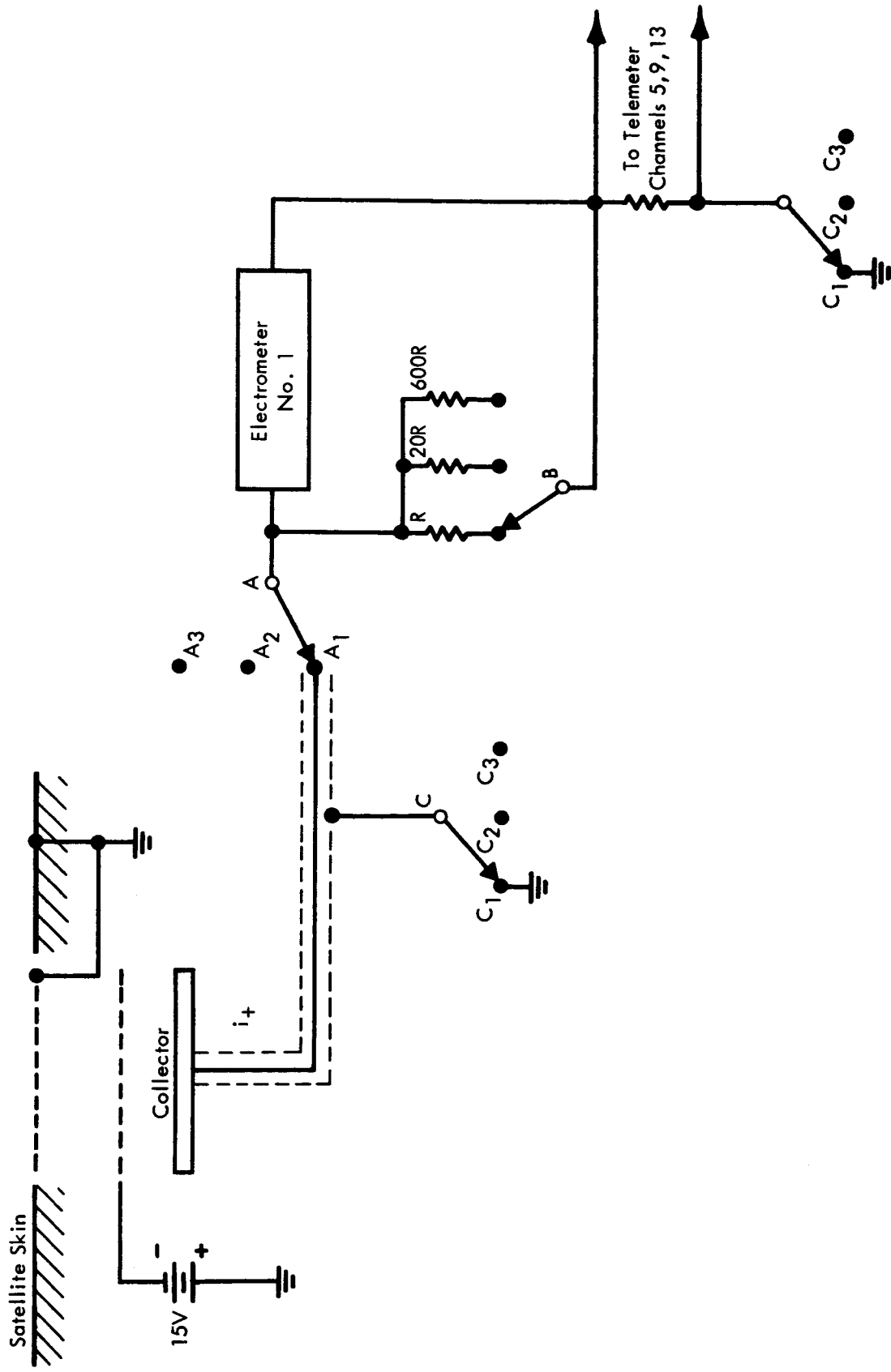


Figure 6. Ion Current Monitor Experiment Explorer VIII Satellite

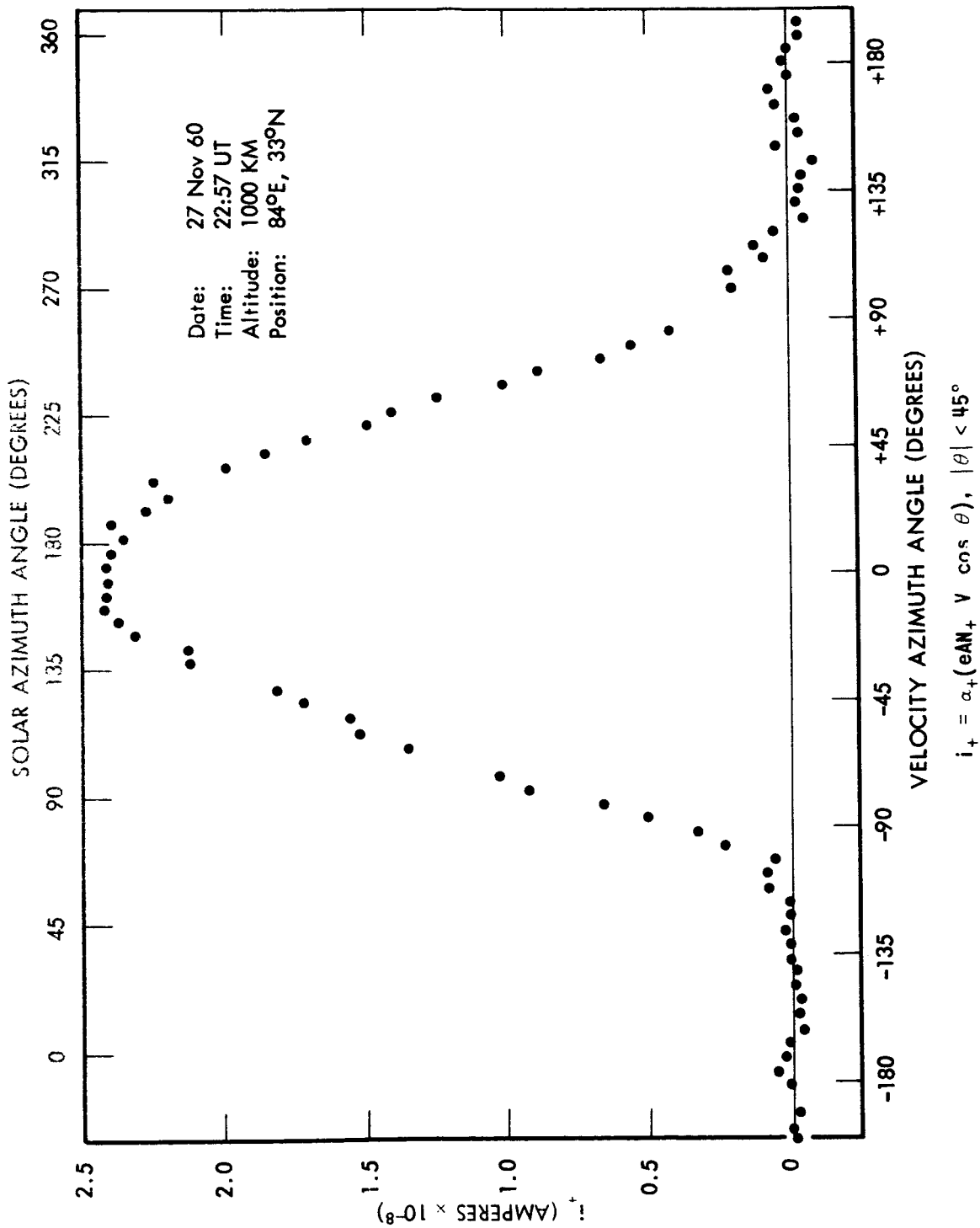


Figure 7. Ion Current as a Function of Aspect, Explorer VIII Satellite.

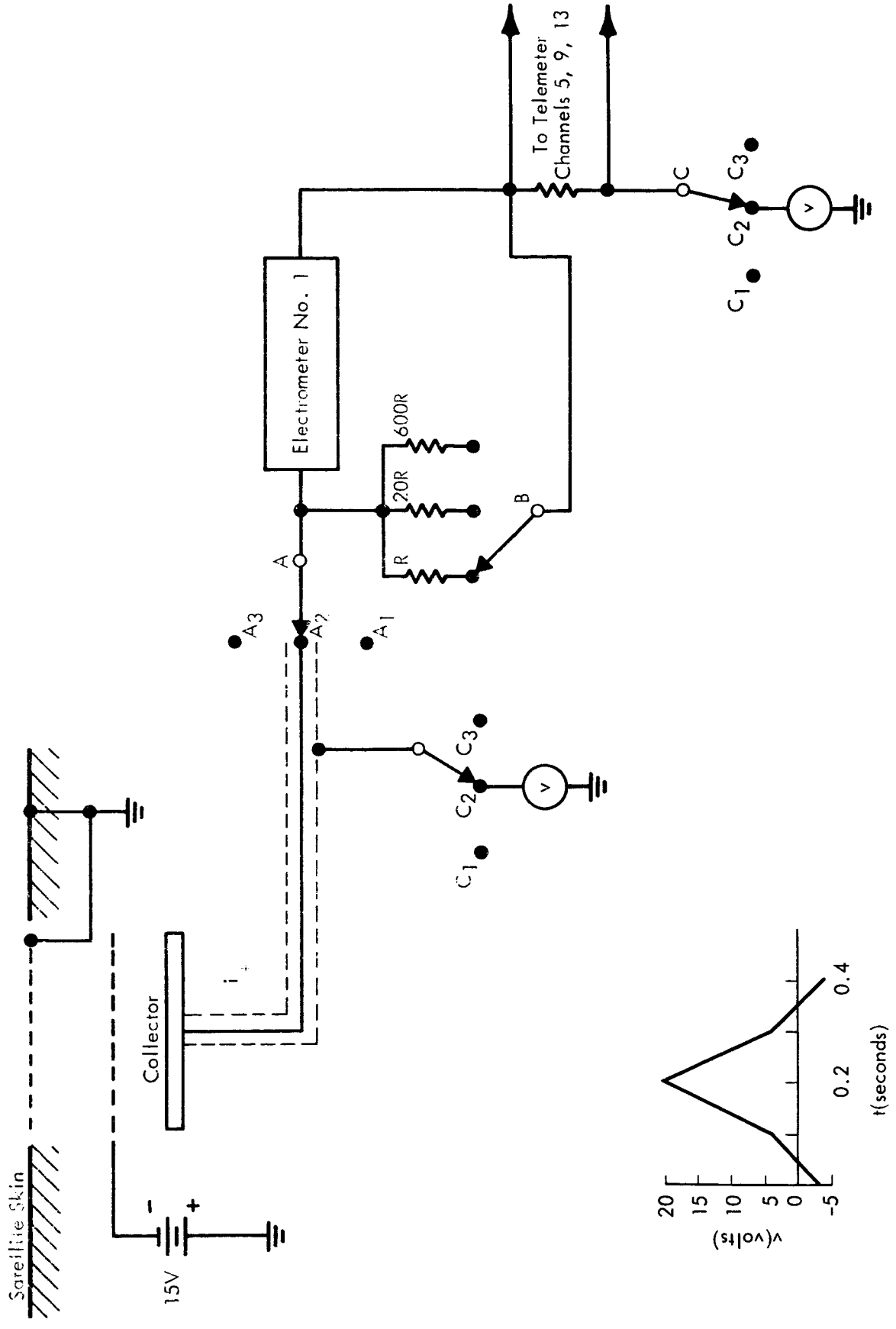
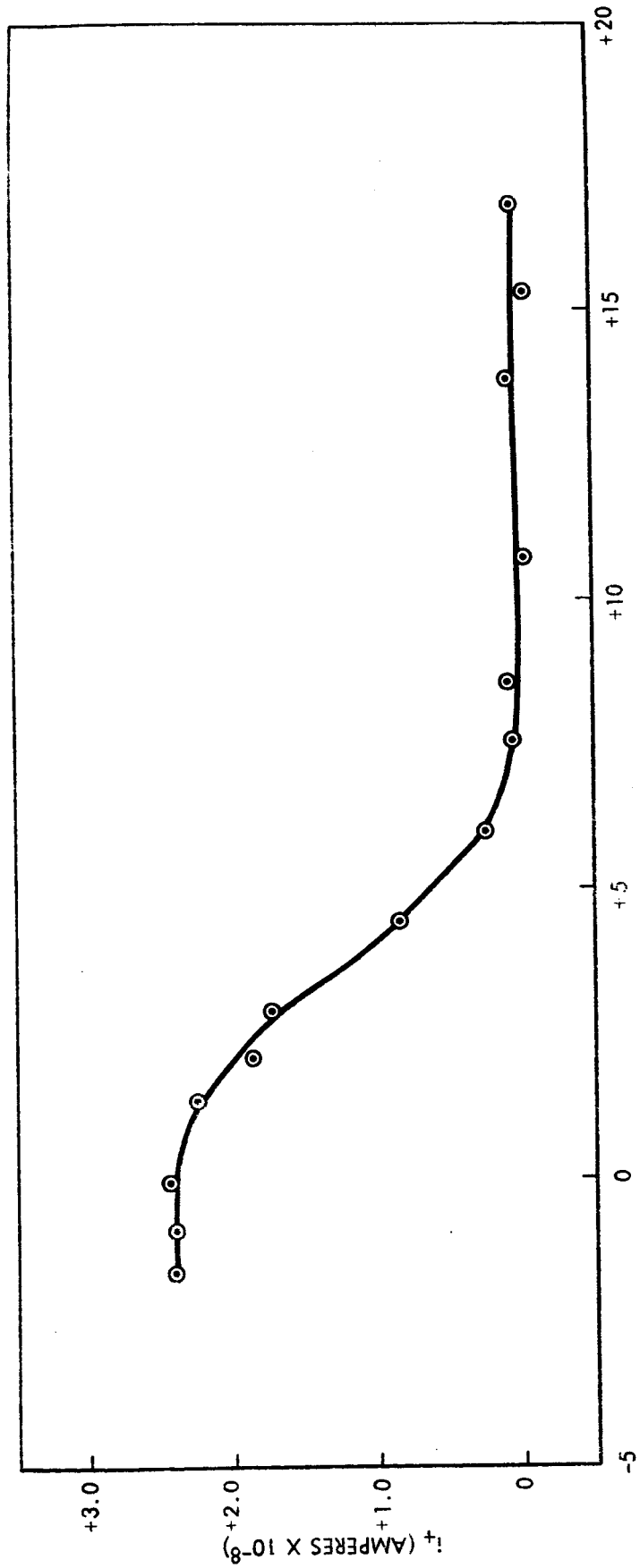


Figure 8. Retarding Potential Experiment, Explorer VIII Satellite.



COLLECTOR-TO-SATELLITE POTENTIAL (VOLTS)

Figure 9. Typical Volt-Ampere Curve, Retarding Potential Experiment.

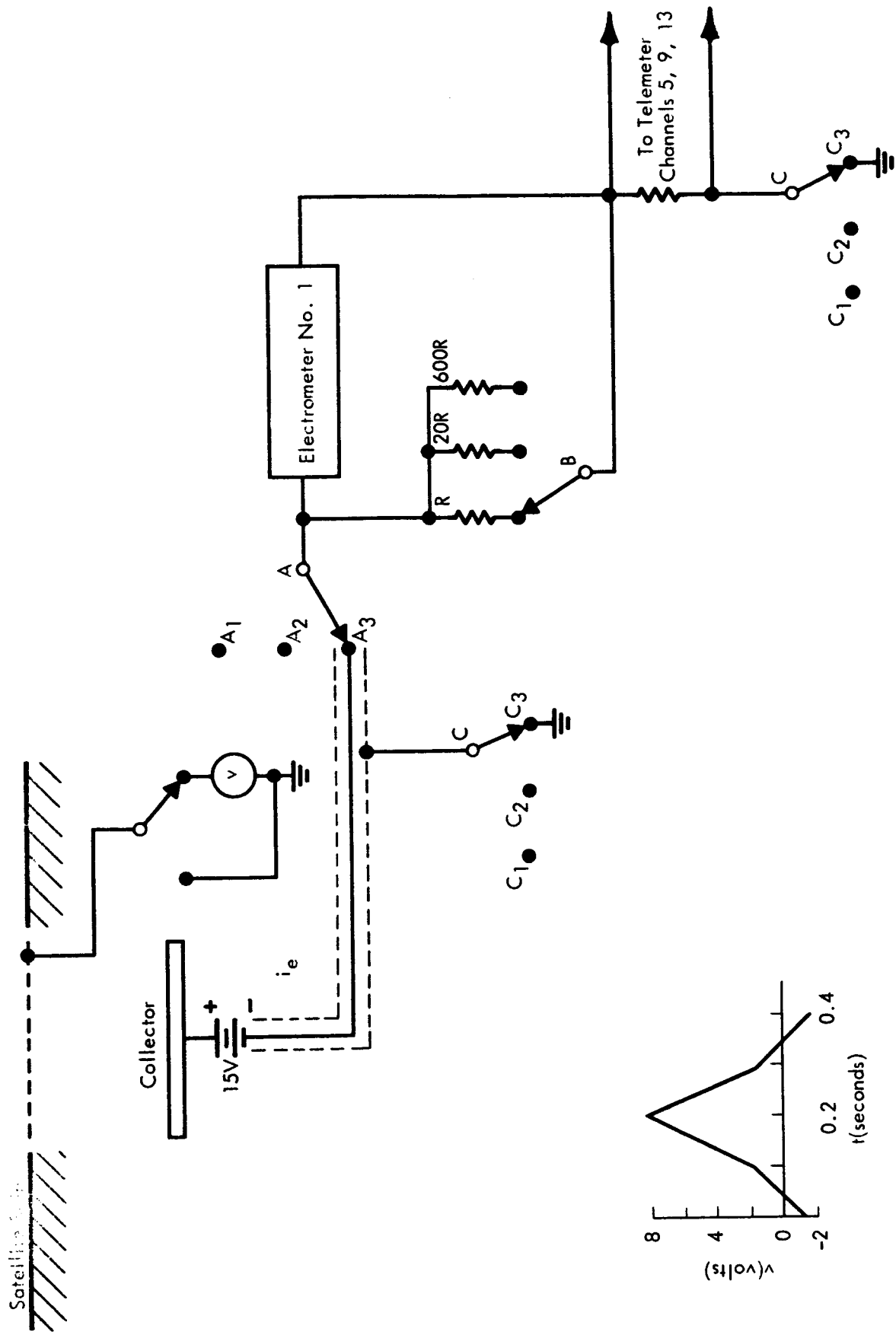


Figure 10. Two-Element Electron Temperature Probe, Explorer VIII Satellite.

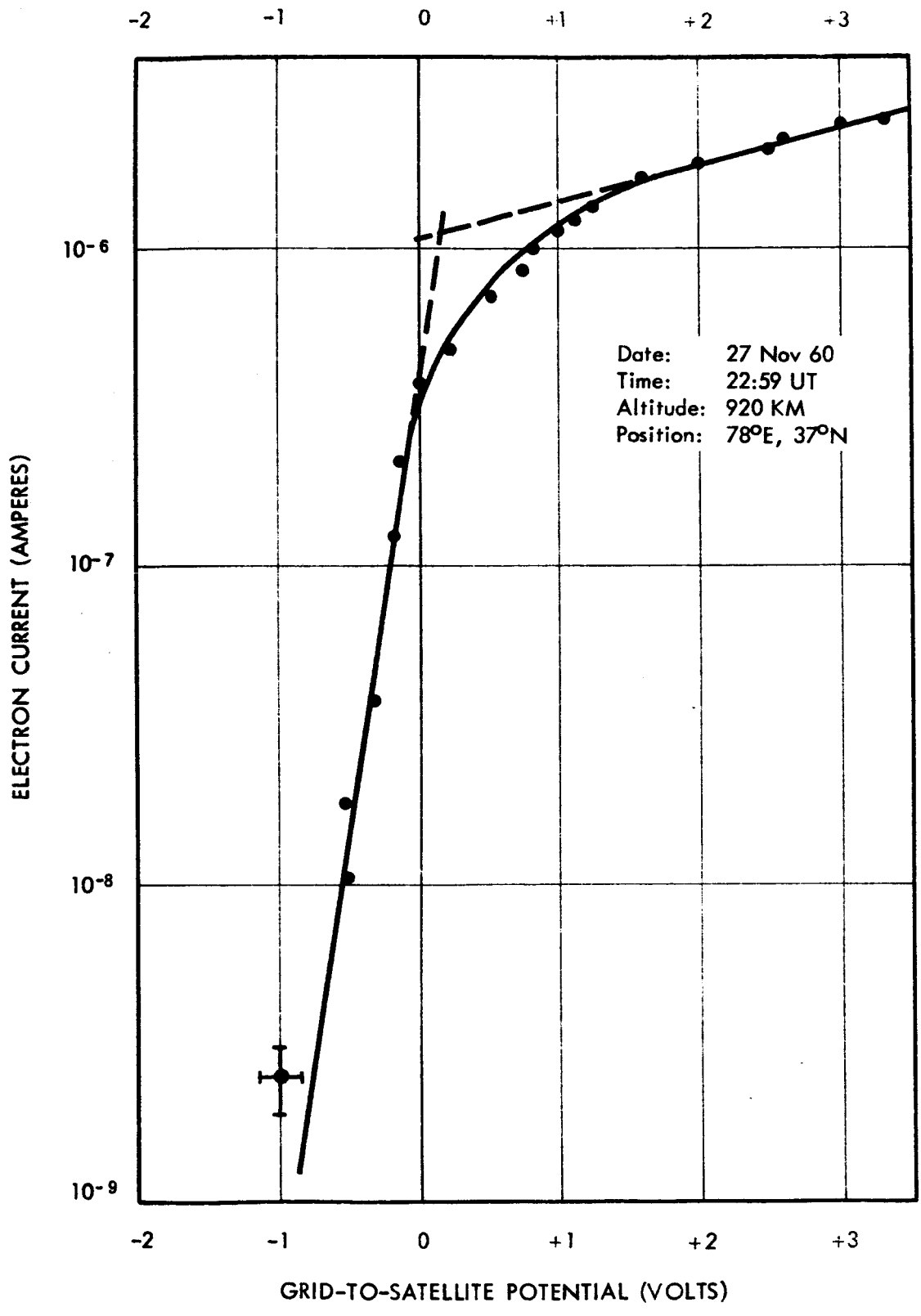


Figure 11. Typical Volt-Ampere Curve, Two-Element Electron Temperature Probe.

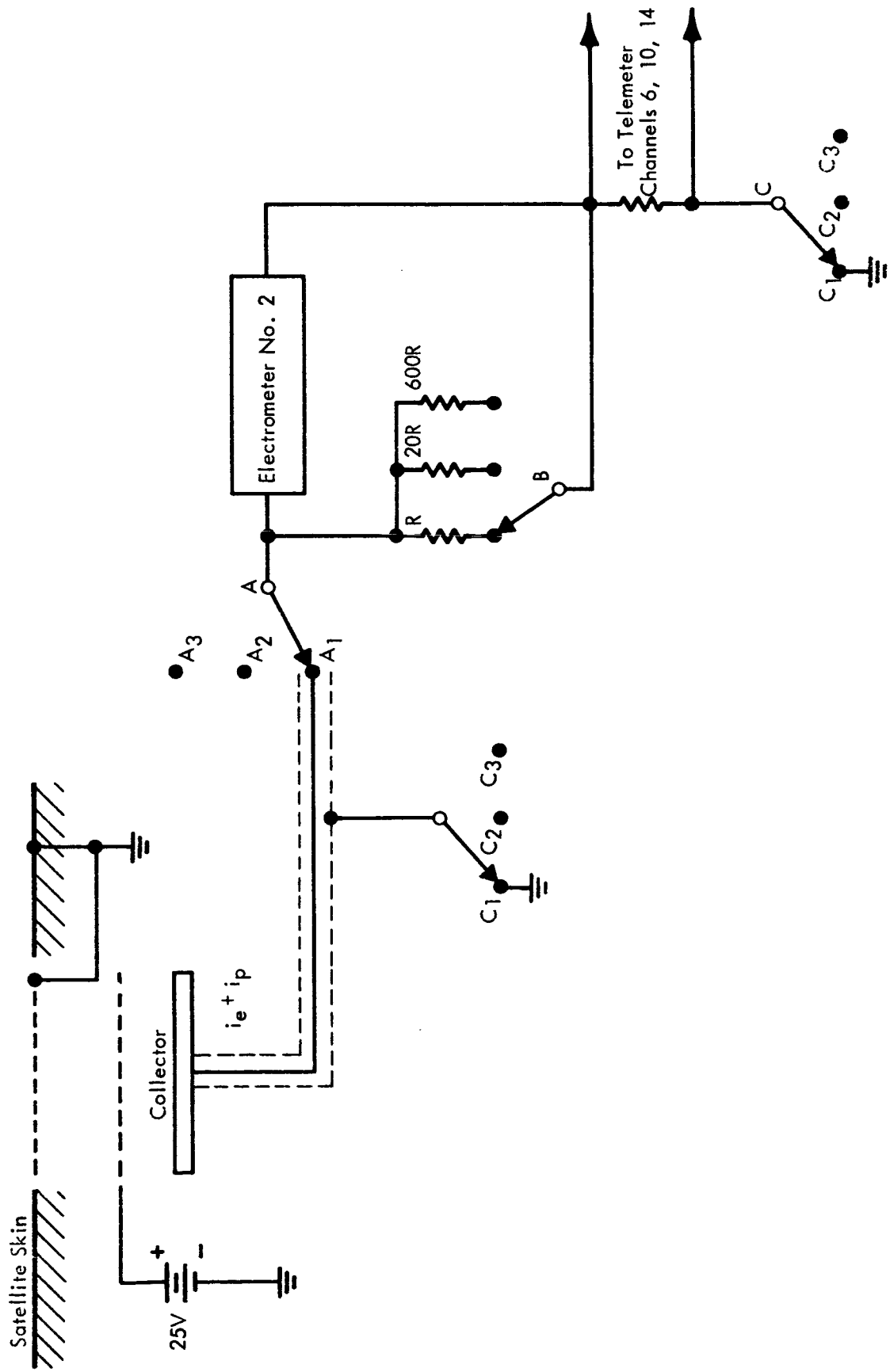


Figure 12. Electron Current Monitor Experiment, Explorer VIII Satellite.

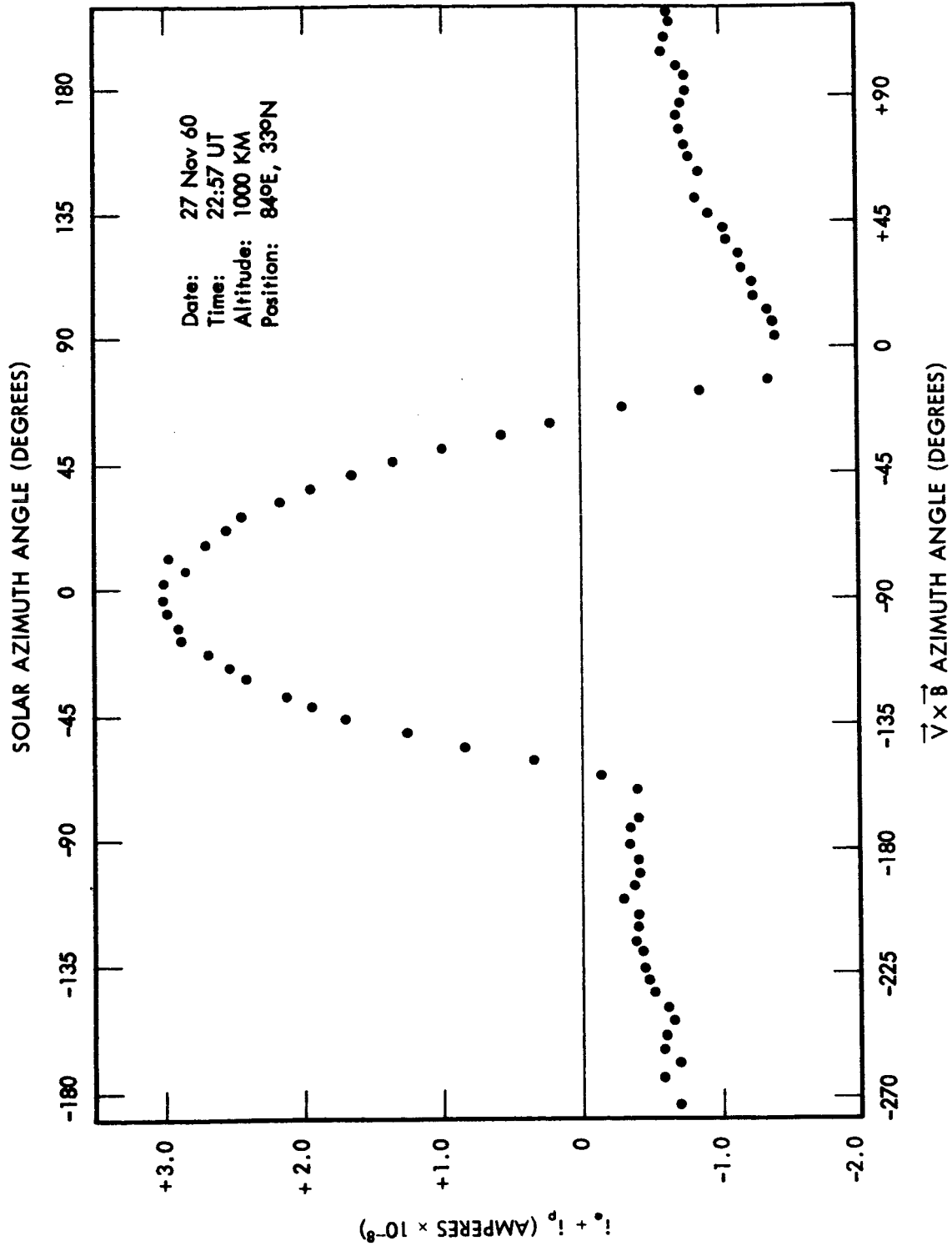


Figure 13. Electron Current as a Function of Aspect, Explorer VIII Satellite.

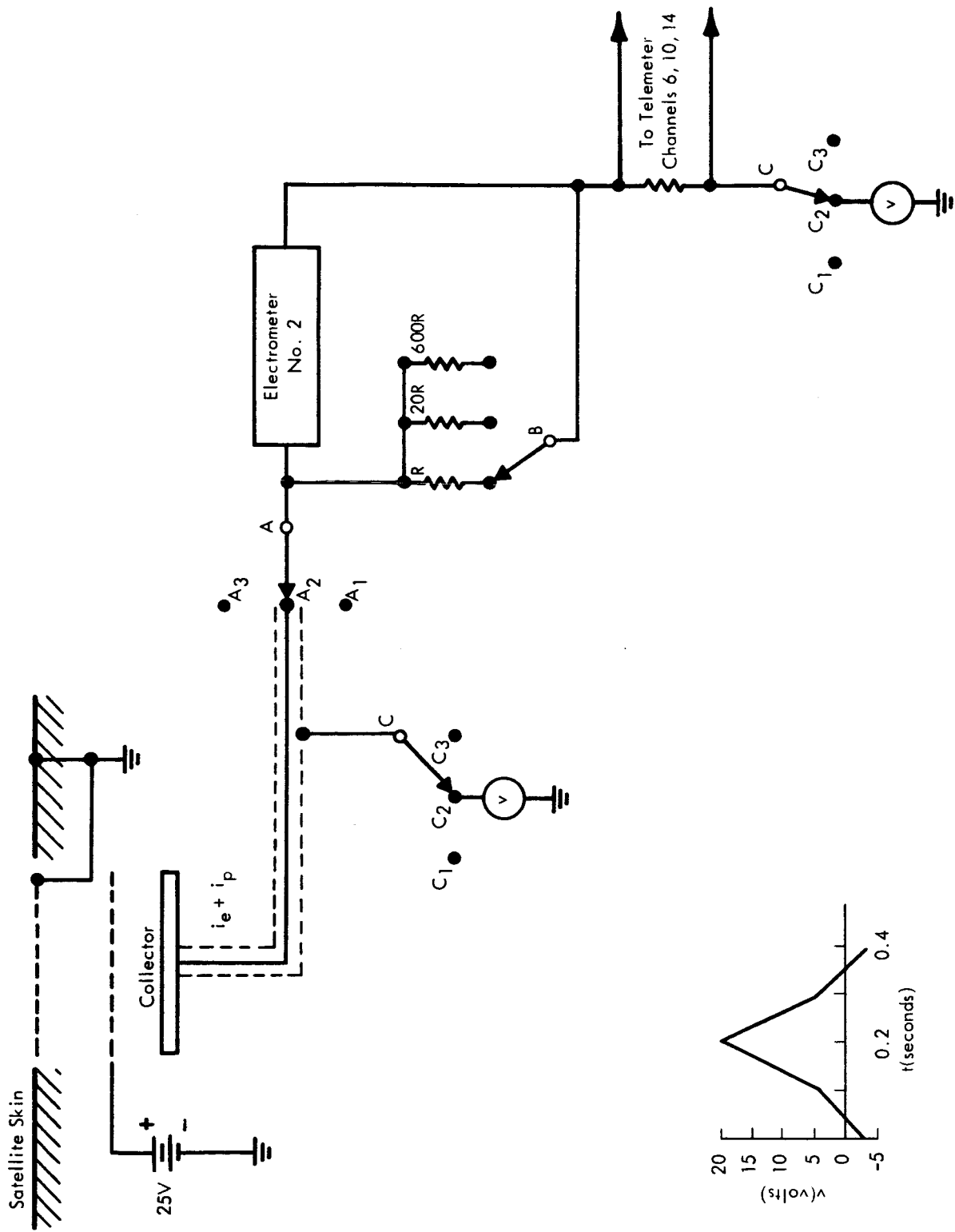


Figure 14. Three-Element Electron Temperature Probe, Explorer VIII Satellite.

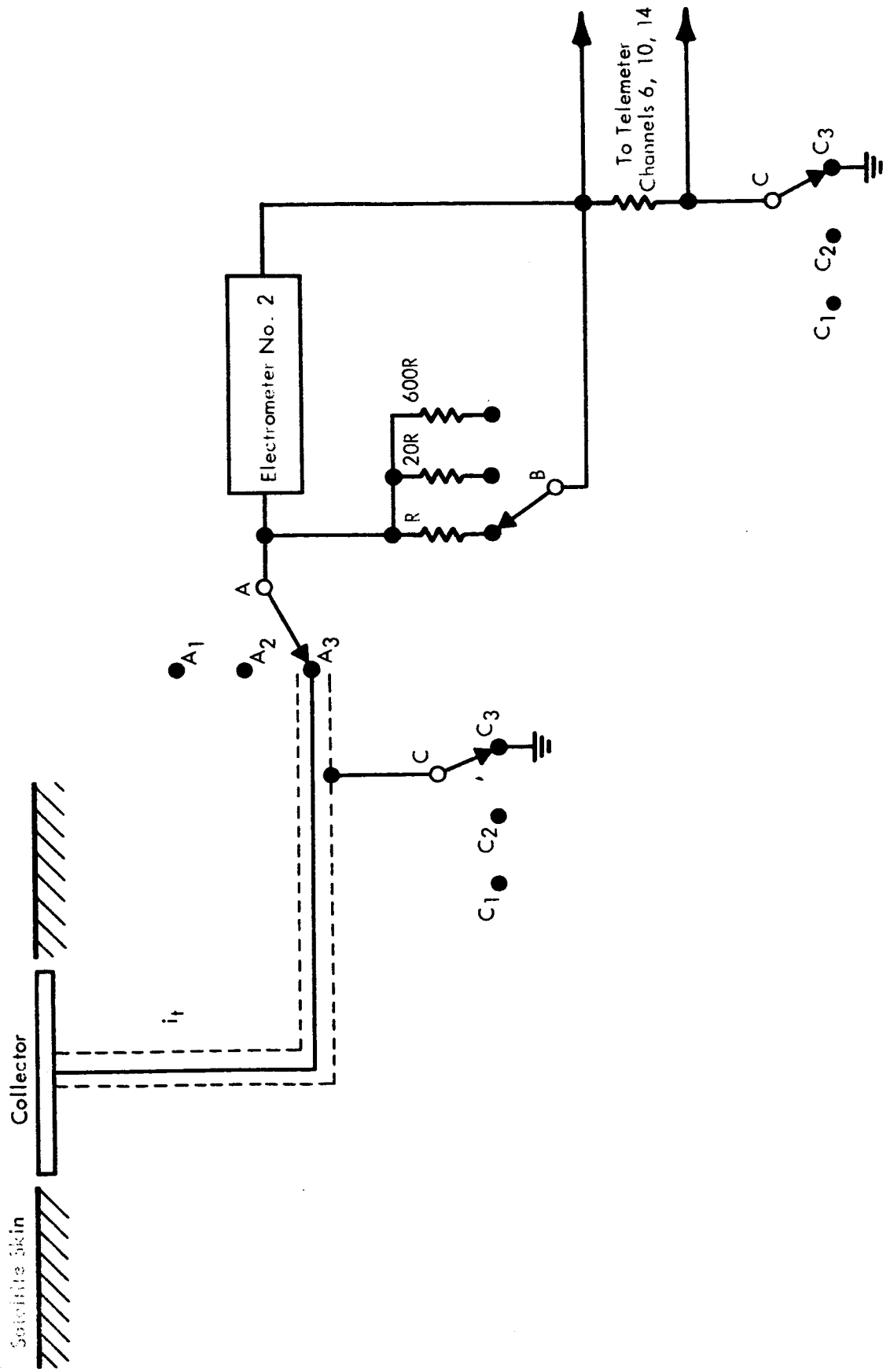


Figure 15. Total Current Monitor Experiment, Explorer VIII Satellite.

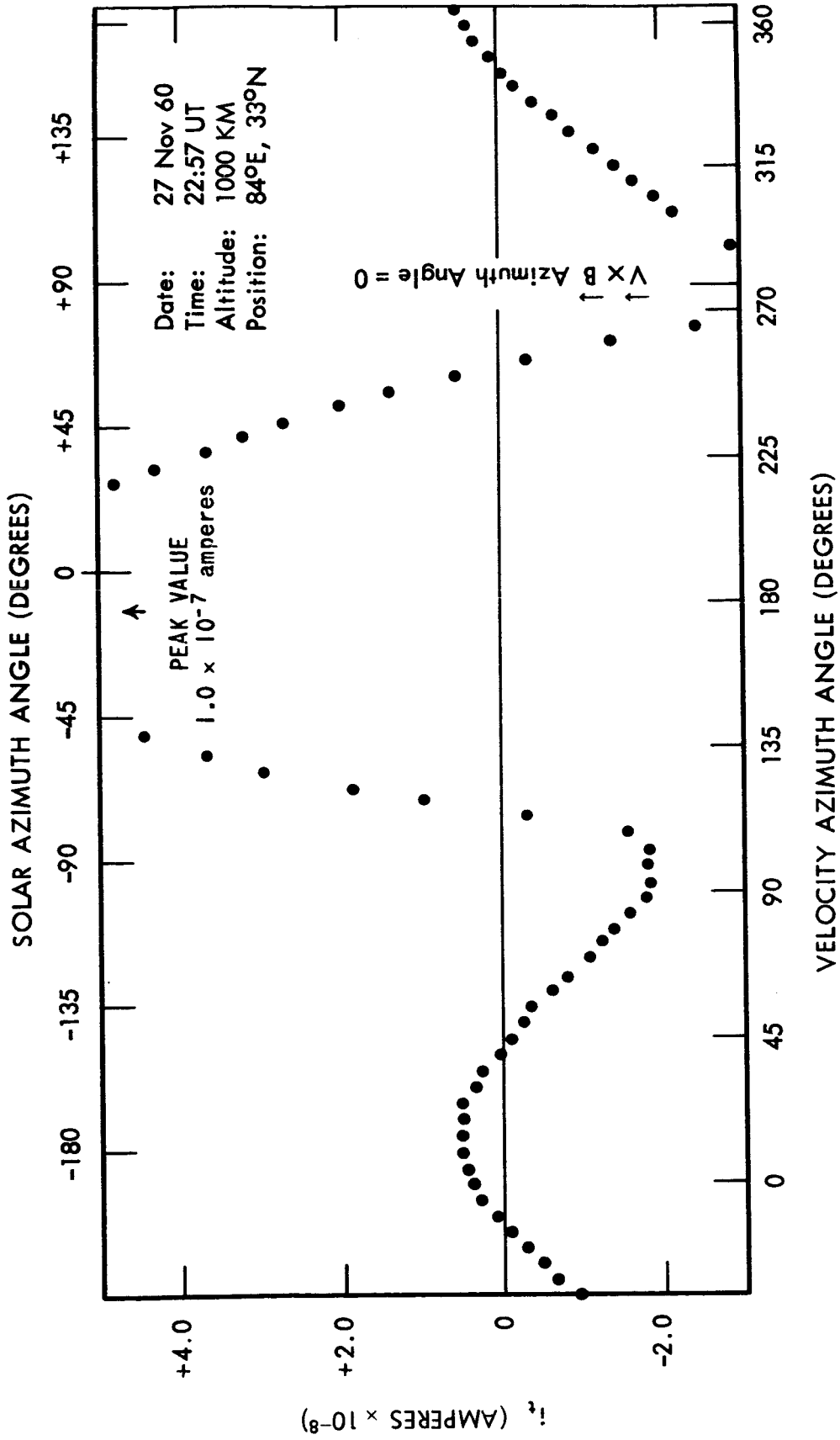


Figure 16. Total Sheath Current as a Function of Aspect, Explorer VIII Satellite.

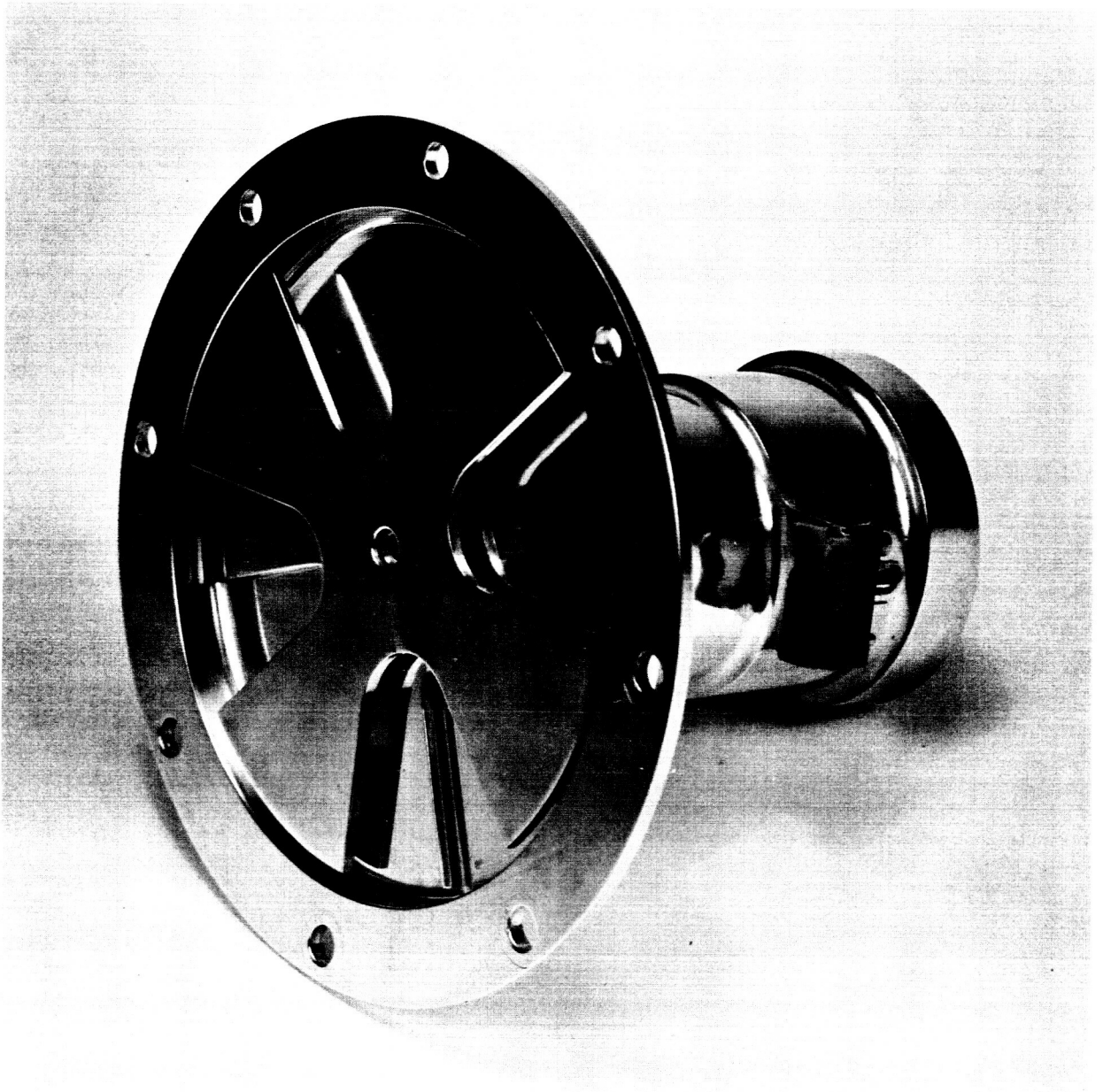


Figure 17. Electric Field Meter, Explorer VIII Satellite.

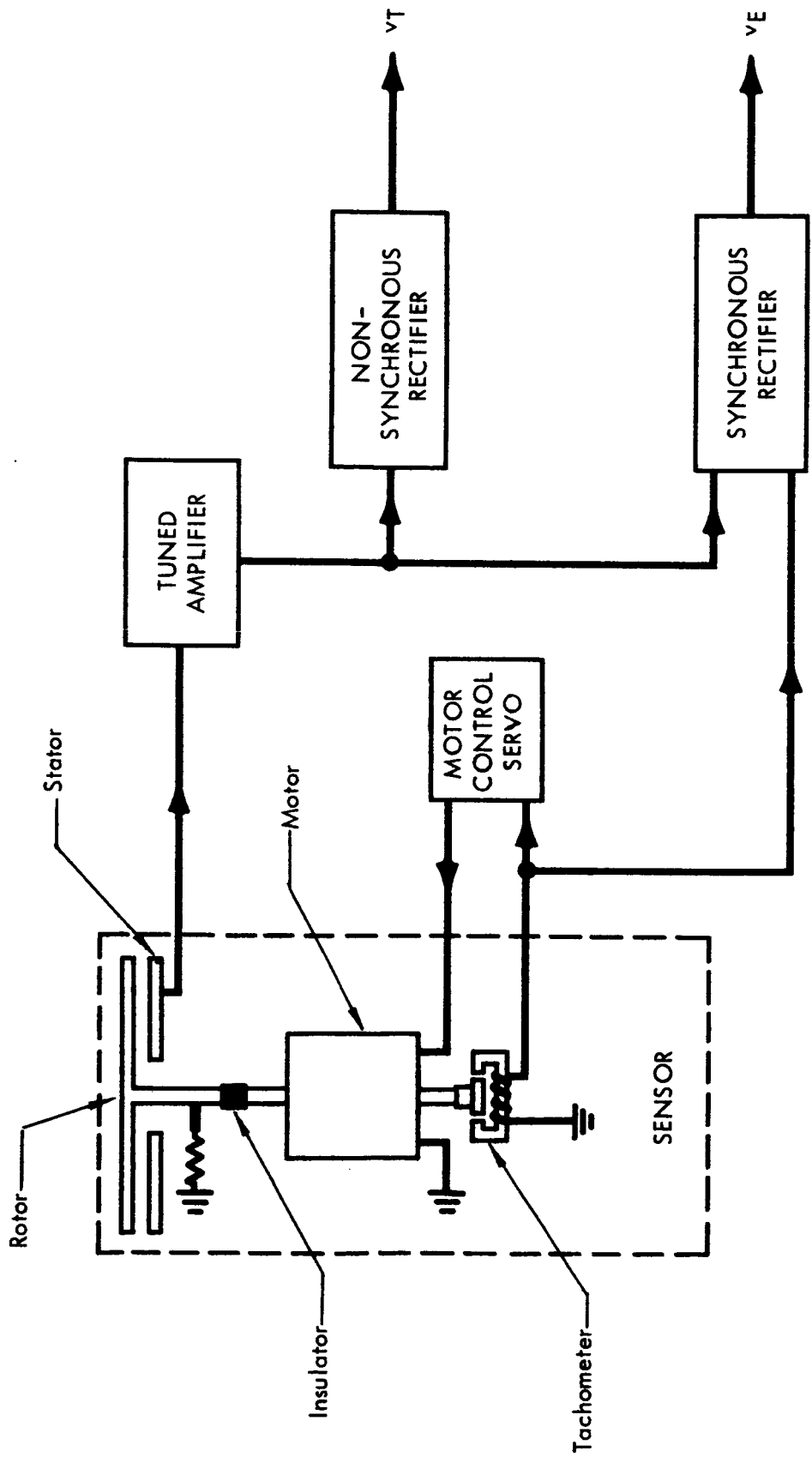


Figure 18. Block Diagram of Electric Field Meter Experiment

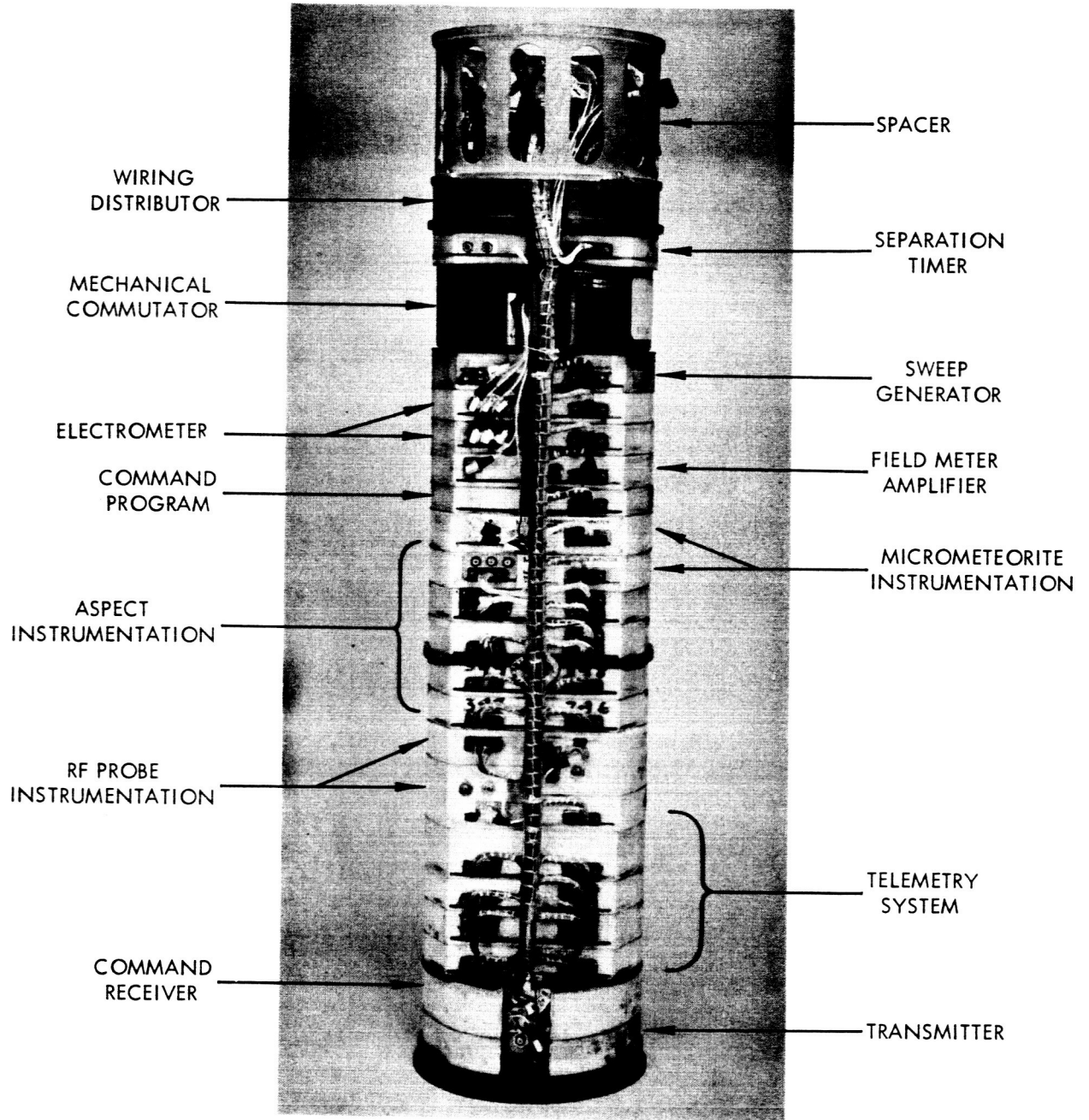


Figure 19. Instrumentation Column.

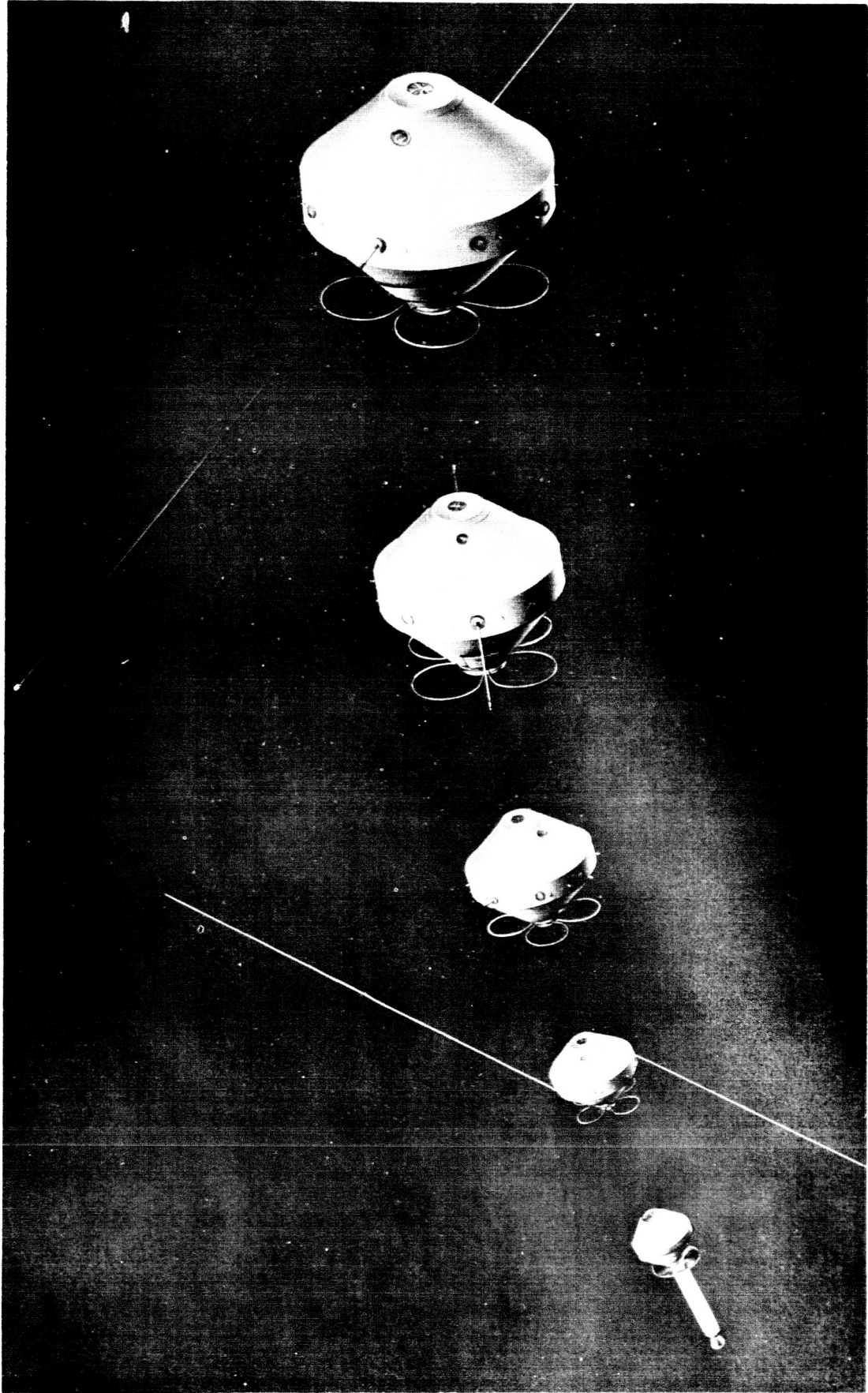


Figure 20. Orbital Injection Sequence, Explorer VIII Satellite.

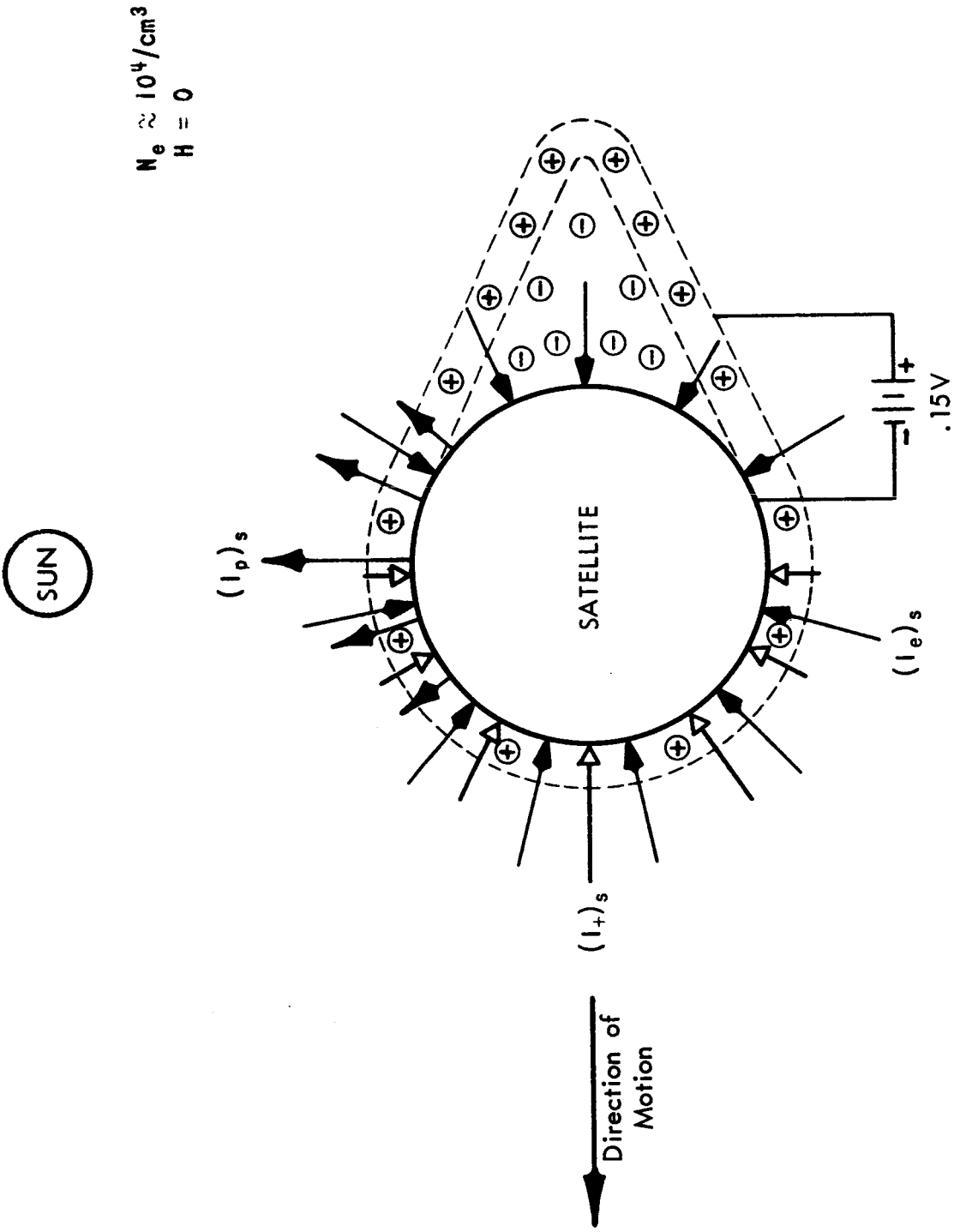


Figure 21. Qualitative Satellite Sheath Model Postulated from Experimental Data.

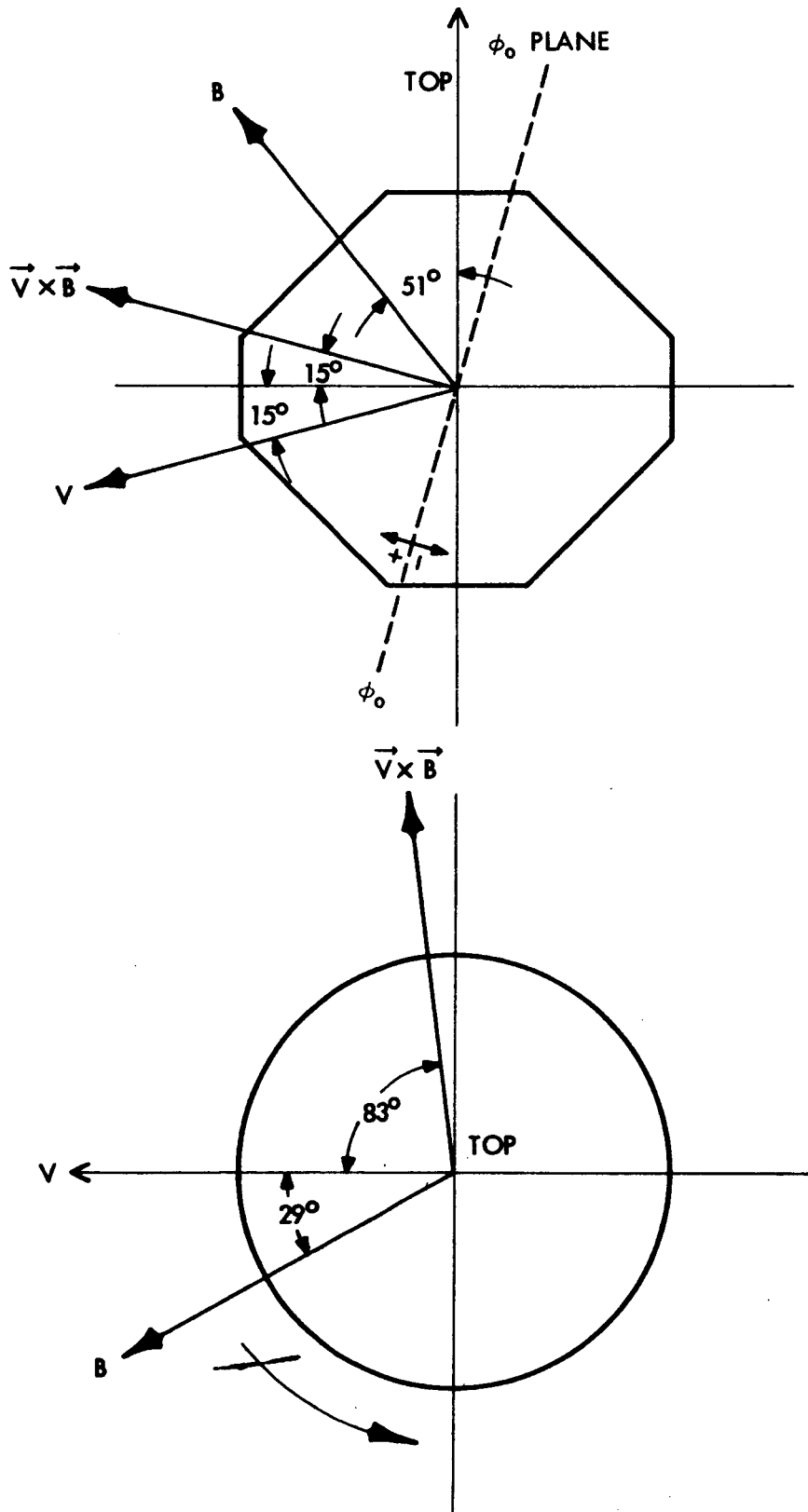


Figure 22. Orientation of Satellite With Respect to Magnetic and Velocity Vectors.

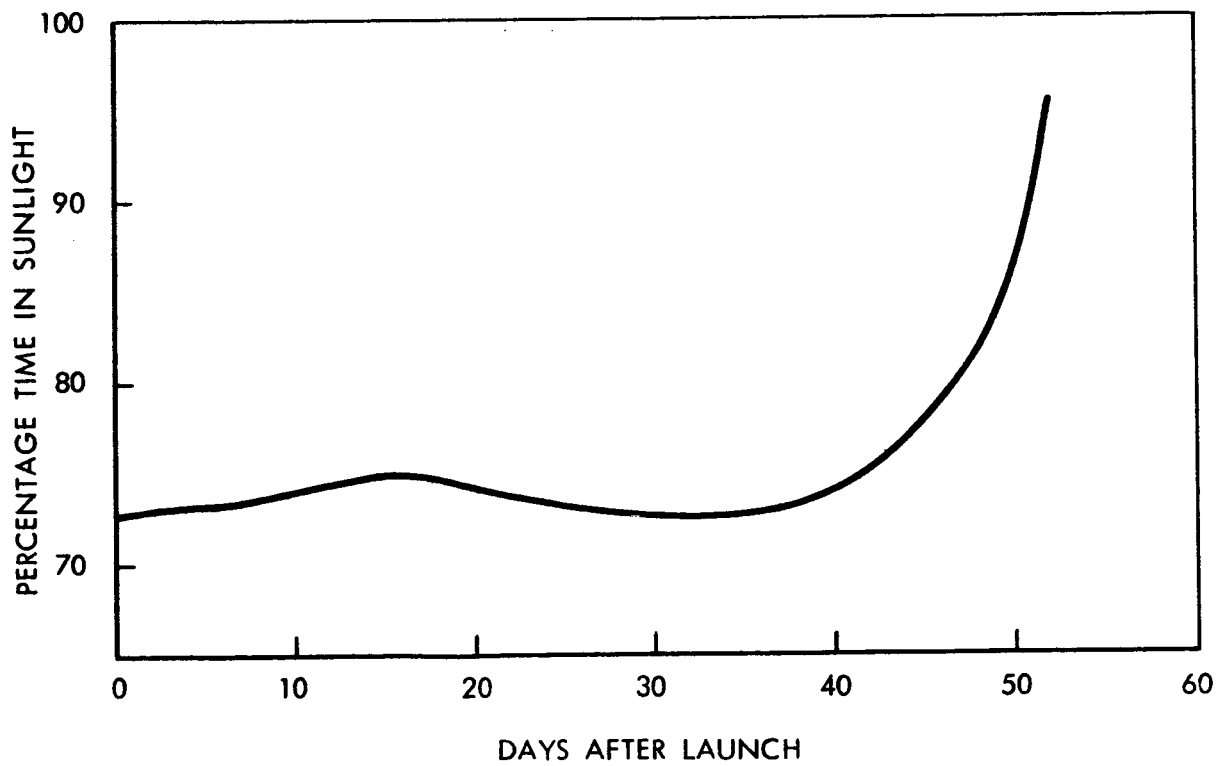
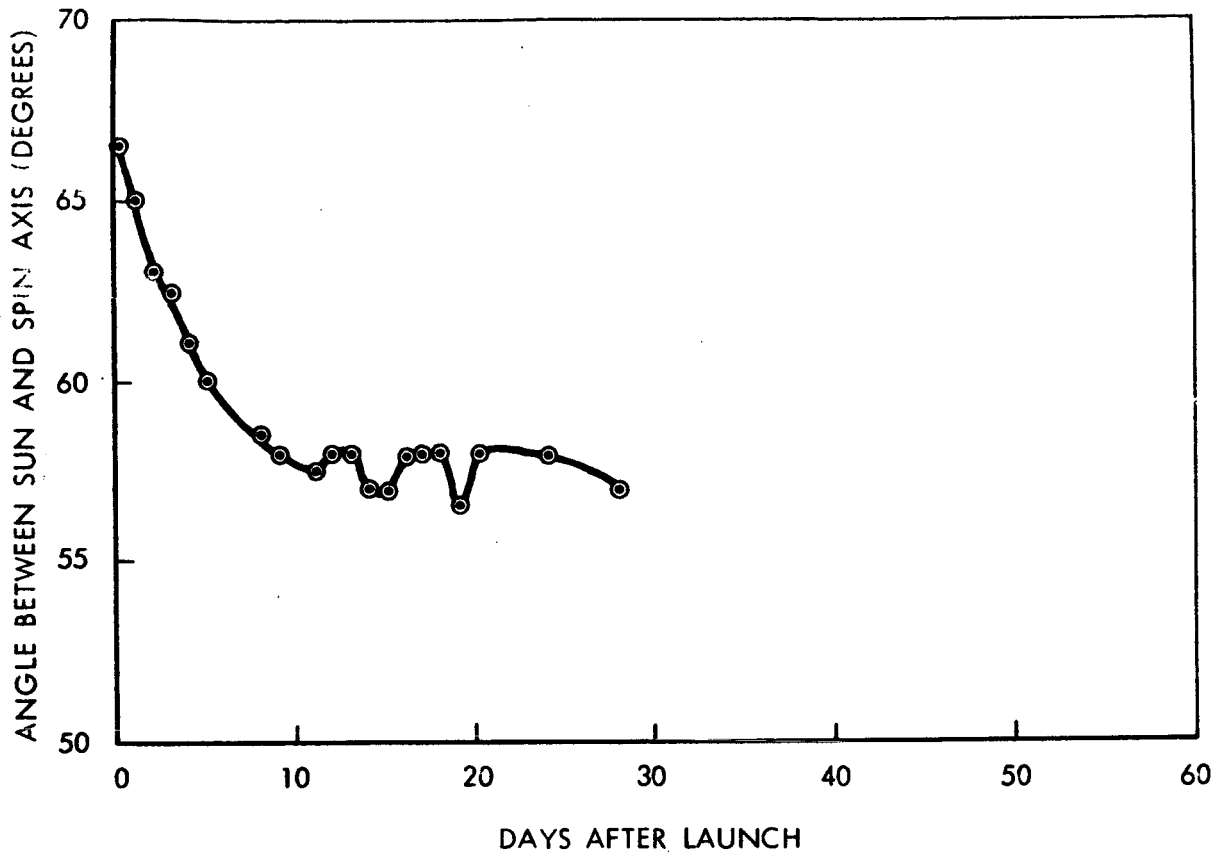


Figure 23. Solar Orientation, Explorer VIII Satellite.